



A hybrid kinetic–fluid model for solving the Vlasov–BGK equation

Nicolas Crouseilles^{a,b,*}, Pierre Degond^a, Mohammed Lemou^a

^a *Mathématiques pour l'Industrie et la Physique, CNRS UMR 5640, Université Paul Sabatier – Toulouse 3, UFR MIG, 118 route de Narbonne, F-31062 Toulouse Cedex 4, France*

^b *CEA-CESTA (DEV/SIS), BP2 33114 Le Barp, France*

Received 14 April 2004; received in revised form 5 August 2004; accepted 16 September 2004

Abstract

Our purpose is to derive a model for charged particles which combines a kinetic description of the fast particles with a fluid description of the slow ones. In a previous paper, a similar model was derived from a kinetic BGK equation that uses a constant relaxation time and does not include the effect of an electric field. In this paper, we consider a more general kinetic equation including an electric field and a varying relaxation time. Fast particles will be described through a collisional kinetic equation of Vlasov–BGK type while thermal particles will be modeled by a hydrodynamic model. Then, we construct a numerical scheme for this model and validate the approach by presenting various numerical tests. © 2004 Elsevier Inc. All rights reserved.

Keywords: Vlasov equation; Euler equations; Entropy minimization principle; Kinetic–hydrodynamic coupling; Numerical schemes

1. Introduction

Numerical simulations have become a very important tool to study complex problems in plasma physics. Consequently, the description of the motion of charged particles arose as a crucial problem. Kinetic models of Boltzmann type and, on the other hand, macroscopic models such as hydrodynamic ones are commonly used in plasma physics. Even if hydrodynamic models are sufficiently accurate to describe many observed phenomena, however, for some of them, a fluid treatment is inadequate. Thus, one must resort to a kinetic model to overcome the insufficiency of the hydrodynamic models. Nevertheless, the numerical simulations of kinetic models are very prohibitive in terms of both CPU time and memory storage. Thus, intermediate models or hybrid approaches have been recently proposed; these approaches appear as a good compromise

* Corresponding author. Tel.: +5 61 55 76 45; fax: +5 61 55 83 85.

E-mail address: crouseilles@mip.ups-tlse.fr (N. Crouseilles).

between physical accuracy and a low computational cost. This paper is a contribution in this direction. Indeed, we derive a hybrid kinetic–fluid model describing the evolution of slow particles by means of a hydrodynamic (or fluid) model, and restricting the use of the kinetic model to the modelling of fast particles.

In a previous paper ([13], see also [12]), the hybrid model was derived in a rarefied gas dynamics context. A transport kinetic equation coupled with a BGK collision operator was considered as our basic model; besides, a constant collision frequency was taken into account. This simple framework enabled us to make rather exhaustive comparisons between the hybrid model, the full kinetic BGK model and the Euler equations. In the present work, we study the evolution of charged particles, so that the basic kinetic model used in [13] and [14] has to be enriched. Two kinds of improvements are performed. On the one hand, we introduce a given or self-consistent electric field (according to the considered case), which represents a wide range of applications in plasma physics. On the other hand, binary collisions between charged particles have to be considered. The simple BGK collision operator used in [14] with constant collision frequency cannot accurately describe such collisions. Usually, the Fokker–Planck–Landau (FPL) collision operator is the common collision model in plasma physics. Classically, the FPL operator is obtained as a remedy to the loss of finiteness of the Boltzmann operator for long-range Coulomb interaction (see [16,21]). It takes the form of a nonlinear partial integro-differential operator whose direct numerical implementation is very expensive and difficult. Consequently, a simpler relaxation time model of BGK type (intended to approximate the FPL operator) is considered in this paper. A collision frequency ν depending on time, space and velocity is computed from the FPL operator using results in [19] for instance. The so-obtained frequency behaves like $|v|^{-3}$ for large particle velocities v which corresponds to the usual behaviour for Coulombian interactions between charged particles (see [2]). On the basis of these two investigations (electric field and collision frequency), a physically realistic numerical code for one-dimensional plasmas has been developed.

Following the methodology introduced in [12] and developed in [13,14], we derive a hybrid kinetic–fluid model based on a domain decomposition method in the velocity variable. We consider a set of particles as described by a distribution function $f = f(t, x, v)$, where $t \in [0, +\infty[$, $x \in \Omega$ and $v \in \mathbb{R}^3$ denote time, position and velocity, respectively, and Ω is a bounded subdomain of \mathbb{R}^3 . The quantity $f(t, x, v) dx dv$ represents the number of particles at time t in an elementary volume $dx dv$ in the phase space around (x, v) . Before defining the model satisfied by f , let us introduce the expression of a Maxwellian \mathcal{M}

$$\mathcal{M}(v) = \exp\left(-\frac{\rho}{RT} - \frac{|v|^2/2 - u \cdot v}{RT}\right), \tag{1.1}$$

where $\rho = \rho(t, x)$, $u = u(t, x)$, $T = T(t, x)$ (the chemical potential, the mean velocity and the temperature of \mathcal{M}) are the parameters of \mathcal{M} ; R is the gas constant. The evolution of f is governed by a kinetic equation which we consider as our starting point for the derivation of the hybrid model

$$\frac{\partial f}{\partial t} + v \cdot \nabla_x f + \frac{e}{m} E \cdot \nabla_v f = \nu(\mathcal{M}_{[f, \nu]} - f), \tag{1.2}$$

where $E = E(t, x)$ is a given electric field, m the mass of the particle, e the unit charge and $\nu = \nu(t, x, v)$ is a collision frequency, depending on time, space and velocity. Moreover, $\mathcal{M}_{[f, \nu]}$ has the Maxwellian form (1.1); its parameters ρ_ν , u_ν , T_ν are functions of t and x only and are determined from the moments of νf by the following constraints:

$$\int_{\mathbb{R}^3} \nu f(v) \begin{pmatrix} 1 \\ v \\ |v|^2 \end{pmatrix} dv = \int_{\mathbb{R}^3} \nu \mathcal{M}_{[f, \nu]}(v) \begin{pmatrix} 1 \\ v \\ |v|^2 \end{pmatrix} dv. \tag{1.3}$$

This ensures the conservation of the mass, the momentum and the energy of the particles. Within the framework of this paper, we also consider a self-consistent electric field E which evolves through the Poisson equation. Eqs. (1.2) and (1.3) are supplemented with an initial condition $f(t = 0, x, v)$.

Our hybrid model relies on the assumption that the particles can be clearly grouped into two categories. The first category consists of thermal particles, whose distribution function is close to a Maxwellian. The second category is that of suprathermal or energetic particles. Following this assumption, we choose a domain B_1 in velocity space (most often a ball as in [13] or [14]) and we suppose that the distribution function can be approximated by a Maxwellian inside B_1 . Therefore, we make the Ansatz that the solution of (1.2) and (1.3) can be approximated by

$$f(v) = \begin{cases} \mathcal{M}_1(v), & v \in B_1, \\ f_2(v), & v \in B_2 = \mathbb{R}^3 \setminus B_1, \end{cases} \quad (1.4)$$

where \mathcal{M}_1 has the Maxwellian form (1.1) and f_2 is the restriction of f to B_2 . The parameters of \mathcal{M}_1 are (ρ_1, u_1, T_1) and are determined by

$$\int_{B_1} f(v) \begin{pmatrix} 1 \\ v \\ |v|^2 \end{pmatrix} dv = \int_{B_1} \mathcal{M}_1(v) \begin{pmatrix} 1 \\ v \\ |v|^2 \end{pmatrix} dv. \quad (1.5)$$

We must derive a set of fluid equations for (ρ_1, u_1, T_1) from the Vlasov–BGK model (1.2) and (1.3), as well as a kinetic equation for f_2 . The way we achieve this task is the same as in [14]: we take the moment equations of (1.2) and (1.3) on the domain B_1 and close the system by using an entropy minimization strategy [29]. The so-obtained system differs from the hybrid model derived in [14] because of the presence of the electric field. It intervenes in two ways. On the one hand, it plays a part as a source term of the fluid model, as usual in the fluid approximation of plasmas [2,11,26]. On the other hand, its influence together with the variations of the fluid domain in space and time, induces fluxes of particles from B_1 to B_2 and vice versa. These fluxes appear as source and sink terms depending on f_2 in the Euler equations, and as boundary conditions depending on \mathcal{M}_1 at the boundary of B_2 for f_2 . Besides, the electric field is present in the kinetic part of the model.

We shall present a numerical strategy which respects the balance between the two sets of equations. The methodology is mainly the same as in [14]: the basic kinetic equation was discretized following a conservative finite volume method which also preserves the positivity, and the decomposition was performed at the discrete level; the discrete moment equations were obtained for the thermal particles and a discrete entropy minimization principle was used to close these equations. In this paper, the main difference comes from the discretization of the Vlasov equation (the left hand side of (1.2)). To that purpose, we adopt a method which discretizes (1.2) on a phase space grid (see [4,36]). But, both conservation and positivity properties are difficult to obtain due to the projection on the grid. Since the positivity property is crucial in our case to guarantee the existence of the Maxwellians \mathcal{M}_1 and $\mathcal{M}_{[f,v]}$, the scheme has to be positive. Thus, we adopt a first order finite volume method which warrants the strict positivity of the distribution function (at the cost of a restriction on the time step), even if it does not ensure the energy conservation. However, following [14], an algorithm that respects the balance between the kinetic and fluid sets of equations can be obtained. Of course, there exist conservative and positive numerical schemes to approach Vlasov type equations without any restriction on the time step (see [24]), but a simpler scheme is chosen here.

In this paper, we try to demonstrate the validity of the hybrid approach by comparing it on the one hand to the kinetic model of BGK type from which the hybrid model can be derived, and on the other hand to the Navier–Stokes equations. To that purpose, various numerical tests have been implemented to describe the evolution of charged particles in the one dimensional case in space and velocity. These numerical tests deal with various plasma physics situations: electronic shock waves, Landau damping, ion acoustic waves or deceleration of an electron beam. Our results are also compared to analytical or literature results, according to the test case.

We now outline some similar approaches in the literature. This approach was first developed for diffusion equations in [12], and for hydrodynamic equations in [13,14]. It bears some similarities with the so-called δf method ([1,35,7]). Most hybrid kinetic–fluid approaches used so far are based on a domain-decomposition in position space: a fluid model is used except in specific regions where the flow is supposed to be far from equilibrium, and where a kinetic model is used (see [5,27,28] for the gas dynamics context and [6,20,31] for the plasmas or [17] for the semiconductors). A smooth transition between the two models can also be envisaged like in [18]. Thus, one uses hybrid codes: a kinetic solver and a hydrodynamic solver are used in different regions of the flows.

The remainder of the paper is organized as follows. In a first part, we derive the hybrid model taking account of a given electric field and a varying collision frequency. Then, we present the numerical scheme allowing us to discretize the hybrid model. Before concluding, various numerical tests coming from plasma physics are presented to validate the approach.

2. Derivation of the hybrid model

This section is devoted to the derivation of the hybrid model describing the evolution of charged particles in a collisional plasma. The starting point of the methodology is the collisional kinetic equation (1.2) and (1.3). This model is a simplified one which allows us to make the derivation of the hybrid model easier. Admittedly, the FPL collision operator is more adapted to describe binary collisions between charged particles, for which the interaction potential is the long-range Coulomb interaction; but its direct numerical implementation is very expensive, in spite of several approaches for reducing its computing cost (see [8]). Consequently, we propose to adopt in this paper a BGK type model which expresses the relaxation towards a local equilibrium. We take into account the FPL collision operator by introducing in (1.2) the collision frequency ν derived from the FPL collision operator. This collision frequency is a function of the velocity (see [2] for instance) and expresses the Coulombian interaction of the particles. Let us denote by $\nu = \nu(|v - u|) \in \mathbb{R}$ (where u is the mean velocity of the considered particles) a collision frequency between the considered particles (like electrons). Some computations which are detailed in Appendix A lead to the following expression of ν :

$$\nu(|v - u|) = C_{\text{FP}} \begin{cases} (4/3)(2\pi)^{-1/2} n / (RT)^{3/2} & \text{if } |v - u| \leq C_0 \sqrt{RT}, \\ 2n / |v - u|^3 & \text{if } |v - u| > C_0 \sqrt{RT}, \end{cases} \tag{2.1}$$

where $C_{\text{FP}} = e^4 \ln A / (8\pi m^2 \epsilon_0^2)$, e is the electric charge, $\ln A$ is the usual Coulomb logarithm and ϵ_0 is the permittivity of free space, m is the mass of the considered particles. Besides, C_0 is chosen such that $\nu(|v - u|)$ is a continuous function of $|v - u|$, i.e.

$$C_0 = \left(\frac{3}{2}\right)^{1/3} (2\pi)^{1/6}.$$

Finally, $R = k_B/m$ is the gas constant associated to the considered particles (where k_B stands for the Boltzmann constant) and n , u , T denote the density, the mean velocity and the temperature of f

$$n = \int_{\mathbb{R}^3} f(v) \, dv, \quad u = \frac{1}{n} \int_{\mathbb{R}^3} v f(v) \, dv, \quad T = \frac{1}{3Rn} \int_{\mathbb{R}^3} |v - u|^2 f(v) \, dv. \tag{2.2}$$

To derive our hybrid model, the starting point is the Vlasov–BGK equation (1.2) and (1.3) where ν is the collision frequency (2.1). Let us now introduce B_1 and B_2

$$B_1 = \left\{ v \in \mathbb{R}^3 \mid |v - \underline{u}| \leq \mathcal{R} \sqrt{RT} \right\}, \quad B_2 = \mathbb{R}^3 \setminus B_1,$$

where \mathcal{R} is a nonnegative constant, \underline{u} and \underline{T} are, respectively, some characteristic velocity and temperature of the plasma. A possible choice can be $\underline{u} = u$ and $\underline{T} = T$, where u and T are given in (2.2). Let us also introduce some notations relative to B_1 and B_2 .

Definition 2.1. For all function $g : \mathbb{R}^3 \rightarrow \mathbb{R}$, we define for $i = 1, 2$

$$g_i(v) = \begin{cases} g(v) & \text{if } v \in B_i, \\ 0 & \text{otherwise.} \end{cases}$$

Our goal is to approximate (1.2) and (1.3) by a kinetic–fluid model. The methodology is the same as in [14] and we refer to it for more details. Let f be a solution to (1.2) and (1.3). Associated to f , we denote by f_2 the unknown of the kinetic part of the hybrid model. On the other hand, the fluid part is a system satisfied by the moments of f on B_1 . If we denote by $m(v)$ the conserved quantities

$$m(v) = (1, v, |v|^2)^T, \tag{2.3}$$

the moments $U_1 = (n_1, P_1, 2W_1)$ of f on B_1 are written

$$\int_{B_1} f(v)m(v) \, dv = \begin{pmatrix} n_1 \\ P_1 \\ 2W_1 \end{pmatrix} = U_1, \tag{2.4}$$

where n_1 is the density, P_1 the momentum and W_1 the total energy of f on B_1 . Finally, we consider the following entropy minimization problem:

$$\left\{ \begin{array}{l} \text{Given } n_1 \geq 0, P_1 \in \mathbb{R}^3, W_1 \geq 0, \text{ find a nonnegative function } \mathcal{M}_1 \text{ on } B_1, \\ \text{realizing the following minimum} \\ \text{Min} \left\{ \int_{B_1} g(v) \log(g(v)) \, dv, g \geq 0, \text{ s.t. } \int_{B_1} g(v)m(v) \, dv = \begin{pmatrix} n_1 \\ P_1 \\ 2W_1 \end{pmatrix} \right\}. \end{array} \right. \tag{2.5}$$

Under some conditions on U_1 , the unique solution of (2.5) is given by a Maxwellian function whose expression is

$$\mathcal{M}_1(v) = \exp(\lambda^1 \cdot m(v)) = \exp(\lambda_0^1 + \lambda_1^1 \cdot v + \lambda_2^1 |v|^2), \tag{2.6}$$

where $\lambda^1 = (\lambda_0^1, \lambda_1^1, \lambda_2^1)^T \in \mathbb{R}^5$ is uniquely determined by the constraints

$$\int_{B_1} \exp(\lambda^1 \cdot m(v))m(v) \, dv = \begin{pmatrix} n_1 \\ P_1 \\ 2W_1 \end{pmatrix}. \tag{2.7}$$

Now, in order to write the hybrid system satisfied by (n_1, P_1, W_1, f_2) , we take the moments of (1.2) on B_1 and close by the Maxwellian (2.6). On B_2 , a kinetic description is kept. In the present case, we obtain the following system on (n_1, P_1, W_1, f_2) :

$$\left\{ \begin{array}{l} \frac{\partial}{\partial t} \begin{pmatrix} n_1 \\ P_1 \\ W_1 \end{pmatrix} + \nabla_x \cdot \begin{pmatrix} \psi_{n_1} \\ \psi_{P_1} \\ \psi_{W_1} \end{pmatrix} = \begin{pmatrix} 0 \\ \frac{e}{m} n_1 E \\ \frac{e}{m} P_1 \cdot E \end{pmatrix} + \begin{pmatrix} n_v^{(1)} - n_{v,1} \\ P_v^{(1)} - P_{v,1} \\ W_v^{(1)} - W_{v,1} \end{pmatrix} + \begin{pmatrix} G_{n_1} \\ G_{P_1} \\ G_{W_1} \end{pmatrix} - \begin{pmatrix} L_{n_1} \\ L_{P_1} \\ L_{W_1} \end{pmatrix}, \\ \frac{\partial f_2}{\partial t} + v \cdot \nabla_x f_2 + \frac{e}{m} E \cdot \nabla_v f_2 = \nu \left((\mathcal{M}_{[\mathcal{M}_1 + f_2, \nu]})_2 - f_2 \right), \text{ on } B_2 \end{array} \right. \tag{2.8}$$

with the boundary condition: $f_2(v) = \mathcal{M}_1(v) \quad \forall v \in \mathbb{S}_+$.

Let us detail the notations used in (2.8). The expressions $(n_v^{(1)}, P_v^{(1)}, W_v^{(1)})$ and $(n_{v,1}, P_{v,1}, W_{v,1})$ are given by:

$$\begin{pmatrix} n_v^{(1)} \\ P_v^{(1)} \\ 2W_v^{(1)} \end{pmatrix} = \int_{B_1} v \mathcal{M}_{[\mathcal{M}_1+f_2, v]} m(v) \, dv, \quad \begin{pmatrix} n_{v,1} \\ P_{v,1} \\ 2W_{v,1} \end{pmatrix} = \int_{B_1} v \mathcal{M}_1(v) m(v) \, dv.$$

The quantities

$$\begin{pmatrix} \psi_{n_1} \\ \psi_{P_1} \\ 2\psi_{W_1} \end{pmatrix} = \int_{B_1} \mathcal{M}_1(v) v m(v) \, dv = \int_{B_1} \mathcal{M}_1(v) \begin{pmatrix} v \\ v \otimes v \\ |v|^2 v \end{pmatrix} \, dv \tag{2.9}$$

are the moment fluxes and $\mathcal{M}_1(v)$ is given by (2.6) and (2.7). The outgoing and incoming semi-fluxes in the fluid equation are defined by:

$$\begin{pmatrix} L_{n_1} \\ L_{P_1} \\ 2L_{W_1} \end{pmatrix} := \int_{\mathbb{S}_+} \vec{F}(v) \cdot \vec{\tau} \mathcal{M}_1(v) m(v) \, dS(v),$$

$$\begin{pmatrix} G_{n_1} \\ G_{P_1} \\ 2G_{W_1} \end{pmatrix} := \int_{\mathbb{S}_-} |\vec{F}(v) \cdot \vec{\tau}| f_2(v) m(v) \, dS(v),$$

where the term

$$\vec{F}(v) = \mathcal{D} \left(\frac{v - \underline{u}}{\mathcal{R}\sqrt{RT}} \right) - \frac{e}{m} E \quad \text{with } \mathcal{D} = \frac{\partial}{\partial t} + v \cdot \nabla_x \tag{2.10}$$

is a force; the first term results from the space and time variations of B_1 whereas the second term is due to the electric field. Now, if we denote by $\mathbb{S}(\underline{u}, \mathcal{R}\sqrt{RT})$ the boundary of B_1 , which, in the case we consider, is a sphere of center \underline{u} and radius $\mathcal{R}\sqrt{RT}$, we can define \mathbb{S}_- and \mathbb{S}_+ as follows:

$$\mathbb{S}_- = \{v \in \mathbb{S}(\underline{u}, \mathcal{R}\sqrt{RT}) \text{ s.t. } \vec{F}(v) \cdot \vec{\tau} < 0\}, \tag{2.11}$$

$$\mathbb{S}_+ = \{v \in \mathbb{S}(\underline{u}, \mathcal{R}\sqrt{RT}) \text{ s.t. } \vec{F}(v) \cdot \vec{\tau} > 0\}, \tag{2.12}$$

where $\vec{\tau}$ is the outward unit normal to $\mathbb{S}(\underline{u}, \mathcal{R}\sqrt{RT})$. Finally, $dS(v)$ is the Euclidean surface element on $\mathbb{S}(\underline{u}, \mathcal{R}\sqrt{RT})$.

3. Numerical schemes for the hybrid model

In this section, we present a numerical scheme for the hybrid model (2.8). The approximation proposed here is mainly the same as [14] and we refer to it for more details. Nevertheless, the hybrid model (2.8) takes account of the effect of an electric field and comprises a velocity derivative. These differences with [14] involve some additional problems. Indeed, it is known that both the conservation of energy and the property of the positivity of the distribution function are difficult to preserve when one approximates the Vlasov equation on a phase space grid. Here, we propose a numerical scheme that ensures the positivity of the distribution function. Indeed, this property of positivity is crucial in our case since it guarantees the Max-

wellian form of the solution to the entropy minimization problem (2.5) (see [32] or [14] for more details). However, the numerical scheme does not ensure the exact conservation of the energy but the perfect balance between the two sets of equations (hydrodynamic and kinetic parts) is preserved at the discrete level.

We start from a fully discretized version of the basic kinetic equation in position, velocity and time. To that purpose, we use a first order finite volume method [23] to approximate the Vlasov–BGK equation (1.2) and (1.3). Then we perform the domain decomposition and pass to the fluid quantities (moments on B_1), directly on the discrete equations. The motion of the ball B_1 , which takes account of the evolution of the mean velocity \underline{u} and the temperature \underline{T} , is performed at the end of each discretization step.

The numerical scheme is presented in one dimension of both space and velocity but can be easily extended to any higher dimensions. For the sake of simplicity, we let $e = m = 1$ in the sequel. We consider a cartesian grid $x_i = i\Delta x$, $v_k = k\Delta v$, $i, k \in \mathbb{Z}$, while $t^n = n\Delta t$ is the time discretization, $n \in \mathbb{N}$. We denote by Δx , Δv and Δt the space, velocity and time steps. We approximate $f(t^n, x_i, v_k)$ by $f_{i,k}^n$ such that

$$f_{i,k}^{n+1} = f_{i,k}^n - v_k^+ \frac{\Delta t}{\Delta x} [f_{i,k}^n - f_{i-1,k}^n] - v_k^- \frac{\Delta t}{\Delta x} [f_{i+1,k}^n - f_{i,k}^n] - E_i^{n,+} \frac{\Delta t}{\Delta v} [f_{i,k}^n - f_{i,k-1}^n] - E_i^{n,-} \frac{\Delta t}{\Delta v} [f_{i,k+1}^n - f_{i,k}^n] + \Delta t v_{i,k}^n [\mathcal{E}_{i,k}^n - f_{i,k}^n], \tag{3.1}$$

where $b^\pm = (b \pm |b|)/2$ for an arbitrary real quantity b , $E_i^n = E(t^n, x_i)$, $v_{i,k}^n = v(t^n, x_i, v_k)$ and $\mathcal{E}_{i,k}^n$ is defined as being the Maxwellian such that

$$\sum_{k \in \mathbb{Z}} v_{i,k}^n \mathcal{E}_{i,k}^n m_k \Delta v = \sum_{k \in \mathbb{Z}} v_{i,k}^n f_{i,k}^n m_k \Delta v \tag{3.2}$$

with $m_k = m(v_k)$

$$m_k = (1, v_k, |v_k|^2). \tag{3.3}$$

Now, in order to decompose the velocity domain, we have to define a discretized version of the ball B_1 . In the remainder of this paper, we shall choose \underline{u} and \underline{T} as the global mean velocity u and temperature T , respectively. They are approximated at point x_i and at time t^n by:

$$\underline{u}_i^n = \frac{P_i^n}{n_i^n}, \tag{3.4}$$

$$\underline{T}_i^n = \frac{2W_i^n n_i^n - (P_i^n)^2}{R(n_i^n)^2}, \tag{3.5}$$

where n_i^n, P_i^n and W_i^n are the mass, momentum and energy at x_i and t^n , and are such that

$$U_i^n = \begin{pmatrix} n_i^n \\ P_i^n \\ 2W_i^n \end{pmatrix} = \sum_{k \in \mathbb{Z}} f_{i,k}^n m_k \Delta v.$$

Then, at position x_i and time t^n , $(B_1)_i^n$ can be approximated by the following discrete set:

$$\mathcal{H}_i^n = \{k \in \mathbb{Z} \text{ s.t. } v_k = k\Delta v \text{ satisfies } |v_k - \underline{u}_i^n| \leq \mathcal{R} \sqrt{R \underline{T}_i^n}\}, \tag{3.6}$$

where \mathcal{R} is an arbitrary nonnegative parameter.

To introduce the moments of a discrete distribution function, let us denote by $g = (g_k)_{k \in \mathbb{Z}}$ an arbitrary sequence. Then, we define the moments of g on \mathcal{H}_i^n by

$$M_i^n(g) = \sum_{k \in \mathcal{K}_i^n} g_k m_k \Delta v$$

and the moments of the shifted sequences $(g_{k \pm 1})_{k \in \mathbb{Z}}$

$$M_{i,\pm}^n(g) = \sum_{k \in \mathcal{K}_i^n} g_{k \pm 1} m_k \Delta v.$$

We also denote by

$$U_{1,i}^n = M_i^n(f_i^n),$$

the discrete moments of $f_i^n = (f_{i,k}^n)_{k \in \mathbb{Z}}$ on the discrete ball; the restriction of $(f_{i,k}^n)_{k \in \mathbb{Z}}$ on $\mathbb{Z} \setminus \mathcal{K}_i^n$ is defined by

$$f_{2,i,k}^n = \begin{cases} f_{i,k}^n & \text{if } k \in \mathbb{Z} \setminus \mathcal{K}_i^n, \\ 0 & \text{otherwise.} \end{cases}$$

We are going to present an algorithm which, from the knowledge of $\mathcal{K}_i^n, U_{1,i}^n, f_{2,i,k}^n$ at time t^n , computes $\mathcal{K}_i^{n+1}, U_{1,i}^{n+1}, f_{2,i,k}^{n+1}$ at time t^{n+1} , based on the moments of (3.1). First, the discrete fluxes on \mathcal{K}_i^n of an arbitrary discrete distribution function $g = (g_k)_{k \in \mathbb{Z}}$ are denoted by

$$\psi_{1,i,\pm}^n(g) = \sum_{k \in \mathcal{K}_i^n} v_k^\pm g_k m_k \Delta v, \tag{3.7}$$

whereas the moments of $v_i^n \mathcal{G}_i^n = (v_{i,k}^n \mathcal{G}_{i,k}^n)_{k \in \mathbb{Z}}$ and of $v_i^n f_i^n = (v_{i,k}^n f_{i,k}^n)_{k \in \mathbb{Z}}$ on \mathcal{K}_i^n are written

$$U_{1,i,v}^n = M_i^n(v_i^n f_i^n), \quad U_{(1),i,v}^n = M_i^n(v_i^n \mathcal{G}_i^n).$$

To close our discrete moment systems, we shall approximate $f_{i,k}^n$ on \mathcal{K}_i^n by the solution $(\mathcal{M}_{1,i,k}^n)_{k \in \mathcal{K}_i^n}$ of the following minimization problem with the prescribed moments $U_{1,i}^n$:

$$\text{Min} \left\{ \sum_{k \in \mathcal{K}_i^n} g_k \log(g_k) \Delta v, \quad g = (g_k)_{k \in \mathbb{Z}}, \quad g_k \geq 0 \quad \forall k \in \mathcal{K}_i^n \text{ s.t. } M_i^n(g) = U_{1,i}^n \right\}. \tag{3.8}$$

This minimization problem is solved in the same way as in [14]. If the prescribed moments $U_{1,i}^n$ are strictly realizable (i.e., $U_{1,i}^n$ is the moment vector of a strictly positive discrete function), $\mathcal{M}_{1,i,k}^n$ has the following Maxwellian form $\mathcal{M}_{1,i,k}^n = \exp(\lambda_{1,i}^n \cdot m_k)$, where $\lambda_{1,i}^n \in \mathbb{R}^3$ is the solution to the discrete moment problem:

$$\sum_{k \in \mathcal{K}_i^n} \exp(\lambda_{1,i}^n \cdot m_k) m_k \Delta v = U_{1,i}^n. \tag{3.9}$$

Now, we first take the moments of Eq. (3.1) on \mathcal{K}_i^n and close the resulting equations using $\mathcal{M}_{1,i,k}^n$. In a following step, we shall “move” the set \mathcal{K}_i^n into a new one, \mathcal{K}_i^{n+1} . Let us introduce the moments $\tilde{U}_{1,i}^{n+1}$ of f_i^{n+1} on the ball \mathcal{K}_i^n

$$\tilde{U}_{1,i}^{n+1} = M_i^n(f_i^{n+1}),$$

as well as the restriction of $f_{i,k}^{n+1}$ onto its complementary $\mathbb{Z} \setminus \mathcal{K}_i^n$

$$\tilde{f}_{2,i,k}^{n+1} = \begin{cases} f_{i,k}^{n+1} & \text{if } k \notin \mathcal{K}_i^n, \\ 0 & \text{otherwise.} \end{cases}$$

If we take the discrete moments of Eq. (3.1) on \mathcal{K}_i^n , and close the resulting moment equations by the solution $\mathcal{M}_{1,i,k}^n \quad \forall k \in \mathcal{K}_i^n$ of the discrete entropy minimization problem (3.8) on the one hand, and take the restriction of Eq. (3.1) on $\mathbb{Z} \setminus \mathcal{K}_i^n$ on the other hand, we obtain:

$$\begin{aligned} \tilde{U}_{1,i}^{n+1} &= U_{1,i}^n - \frac{\Delta t}{\Delta x} \left[\psi_{1,i,+}^n(\mathcal{M}_{1,i}^n) - \psi_{1,i,+}^n(\mathcal{M}_{1,i-1}^n + f_{2,i-1}^n) \right] \\ &\quad - \frac{\Delta t}{\Delta x} \left[\psi_{1,i,-}^n(\mathcal{M}_{1,i+1}^n + f_{2,i+1}^n) - \psi_{1,i,-}^n(\mathcal{M}_{1,i}^n) \right] - \frac{\Delta t}{\Delta v} E_i^{n,+} \left[U_{1,i}^n - M_{i,-}^n(\mathcal{M}_{1,i}^n + f_{2,i}^n) \right] \\ &\quad - \frac{\Delta t}{\Delta v} E_i^{n,-} \left[M_{i,+}^n(\mathcal{M}_{1,i}^n + f_{2,i}^n) - U_{1,i}^n \right] + \Delta t \left[U_{(1),i,v}^n - U_{1,i,v}^n \right], \end{aligned} \tag{3.10}$$

$$\begin{aligned} \tilde{f}_{2,i,k}^{n+1} &= f_{2,i,k}^n - v_k^+ \frac{\Delta t}{\Delta x} \left[f_{2,i,k}^n - (\mathcal{M}_{1,i-1,k}^n + f_{2,i-1,k}^n) \right] - v_k^- \frac{\Delta t}{\Delta x} \left[(\mathcal{M}_{1,i+1,k}^n + f_{2,i+1,k}^n) - f_{2,i,k}^n \right] \\ &\quad - E_i^{n,+} \frac{\Delta t}{\Delta v} \left[f_{2,i,k}^n - (f_{2,i,k-1}^n + \mathcal{M}_{1,i,k-1}^n) \right] - E_i^{n,-} \frac{\Delta t}{\Delta v} \left[(f_{2,i,k+1}^n + \mathcal{M}_{1,i,k+1}^n) - f_{2,i,k}^n \right] \\ &\quad + \Delta t v_{i,k}^n \left[\mathcal{E}_{2,i,k}^n - f_{2,i,k}^n \right]. \end{aligned} \tag{3.11}$$

The next step of the algorithm is to consider the time variations of \mathcal{K}_i^n . To that purpose, we construct $(\tilde{\mathcal{M}}_{1,i,k}^{n+1})_{k \in \mathcal{K}_i^n}$ the discrete distribution solution to (3.8) with the prescribed moments $\tilde{U}_{1,i}^{n+1}$. Then we define an approximation of $f_{i,k}^{n+1}$ for all $k \in \mathbb{Z}$, solution to Eq. (3.1) by $\tilde{f}_{i,k}^{n+1}$ such that

$$f_{i,k}^{n+1} \approx \tilde{f}_{i,k}^{n+1} = \begin{cases} \tilde{\mathcal{M}}_{1,i,k}^{n+1} & \text{if } k \in \mathcal{K}_i^n, \\ \tilde{f}_{2,i,k}^{n+1} & \text{if } k \notin \mathcal{K}_i^n. \end{cases}$$

Hence, the discrete moments of $\tilde{f}_{i,k}^{n+1}$ are an approximation of U_i^{n+1} . At this level, $\underline{u}_i^{n+1}, \underline{T}_i^{n+1}$ and \mathcal{K}_i^{n+1} can then be defined through (3.4) and (3.5) (with n replaced by $n + 1$). The unknowns at the next time step are finally:

$$U_{1,i}^{n+1} = M_i^{n+1}(\tilde{f}_i^{n+1}), \tag{3.12}$$

$$f_{2,i,k}^{n+1} = \tilde{f}_{i,k}^{n+1} \Big|_{\mathbb{Z} \setminus \mathcal{K}_i^{n+1}}. \tag{3.13}$$

Remark 3.1. Let us consider $(f_{i,k}^0)_{i \in I, k \in \mathbb{Z}}$ a strictly positive initial condition where I is the discrete bounded computational domain in space. Moreover, let us denote by \mathcal{K} a bounded discrete velocity domain which is a truncation of \mathbb{Z} . If the following condition on the time step Δt is fulfilled:

$$\Delta t \left(\max_{i \in I, k \in \mathcal{K}} v_{i,k}^n + \frac{1}{\Delta x} \max_{k \in \mathcal{K}} |v_k| + \frac{1}{\Delta v} \max_{i \in I} E_i^n \right) < 1,$$

then the kinetic sequence $(f_{2,i,k}^n)_{n \geq 0}$ defined by the above algorithm satisfies

$$f_{2,i,k}^n > 0 \quad \text{for all } n \geq 0, i \in I, k \in \mathcal{K} \setminus \mathcal{K}_i^n.$$

The proof of this statement is a straightforward generalization of a similar statement (with $E = 0$) proved in [14]. Our time-stepping strategy is based on it.

4. Numerical results

In this section, we present numerical tests to validate the approach. We check our method on one-dimensional numerical tests. Although the collision frequency (2.1) was obtained from a three-dimensional

operator, we shall use it in our one-dimensional simulations. We are aiming at a qualitative rather than quantitative results. For more realistic simulations, fully three-dimensional computations are necessary but are outside the scope of the present work. Numerically, the boundary conditions in space variable are treated by a ghost cell technique or by periodic conditions, according to the test case. In the velocity variable, the distribution function is truncated to zero for large velocities.

4.1. Stationary shock wave without electric field

4.1.1. Plasma context

We study a one-dimensional stationary shock wave (see [3,32]) for electrons. The flow is initialized with two Maxwellian states related by the discrete Rankine–Hugoniot relations (see [32] or [14] for more details). The starting kinetic equation is the following:

$$\frac{\partial f}{\partial t} + v \cdot \nabla_x f = \nu(\mathcal{M}_{[f,\nu]} - f), \tag{4.1}$$

where ν is chosen as in Definition 2.1

$$\nu(|v - u|) = C_{FP} \begin{cases} (4/3)(2\pi)^{-1/2} n / (R_e T)^{3/2} & \text{if } |v - u| < C_0 \sqrt{R_e T}, \\ 2n / |v - u|^3 & \text{if } |v - u| \geq C_0 \sqrt{R_e T}, \end{cases} \tag{4.2}$$

where $C_0 = (3/2)^{1/3} (2\pi)^{1/6}$, and $C_{FP} = e^4 \ln \Lambda / (8\pi m_e^2 \epsilon_0^2)$. We have used the following values for the density $n_L = 7.2857 \times 10^{24} \text{ m}^{-3}$, the mean velocity $u_L = 6.95549 \times 10^5 \text{ m s}^{-1}$, and the temperature $T_L = 293 \text{ K}$, of the upstream flow. We only consider electrons whose mass is equal to $m_e = 9.1 \times 10^{-31} \text{ kg}$. These values yield a shock Mach number equal to 6.

For numerical reasons, we will use dimensionless variables. We choose as units of our problem the mean free path l as unit of length, the thermal velocity $v_0 = \sqrt{R_e T_R}$ (where T_R is the temperature of the downstream flow) as unit of velocity and the collision time $\tau_0 = l/v_0$ as unit of time. We choose the values of l , v_0 and τ_0 as following:

$$l = 5.158 \times 10^{-9} \text{ m}, \quad v_0 = \sqrt{R_e T_R} = 3.49583 \times 10^5 \text{ m s}^{-1}, \quad \tau_0 = l/v_0 = 1.4755 \times 10^{-14} \text{ s}.$$

We obtain the following value for the dimensionless C_{FP} :

$$C'_{FP} = C_{FP} / (l^6 \tau_0^{-4}) = C_{FP} / (l^2 v_0^4) = 15.25.$$

The velocity set extends from $-v_{\max}$ to $v_{\max} = 6$ and the physical space is $[0,50]$. The velocity step Δv is chosen equal to 0.05 whereas $N_x = 200$ points are used in the x variable. The same numerical parameters are used for the kinetic model.

In Figs. 1–3, we present the profiles of the density, the mean velocity and the temperature, as functions of the scaled space. These figures display the results obtained by the full BGK equation (discretized by Eq. (3.1)), by the Navier–Stokes equations (discretized following [16]) and by the hybrid model, for different values of \mathcal{R} ($\mathcal{R} = 0.5, 2$ and 4).

We observe that, for small \mathcal{R} , the hybrid model is closer to the BGK model than to the Navier–Stokes equations, but the shock profiles are stiffer than that of the BGK equation. In this case (small values of \mathcal{R}), our model has an intermediate behaviour between the kinetic model and the Navier–Stokes equations, as could be expected. We also notice that the hybrid model has a better behaviour than the Navier–Stokes equations upstream the shock. Moreover, when \mathcal{R} is large enough, the hybrid model present stiffer shock profiles than the Navier–Stokes ones. Indeed, at large \mathcal{R} , the hybrid model approximates the Euler equations (without diffusion terms).

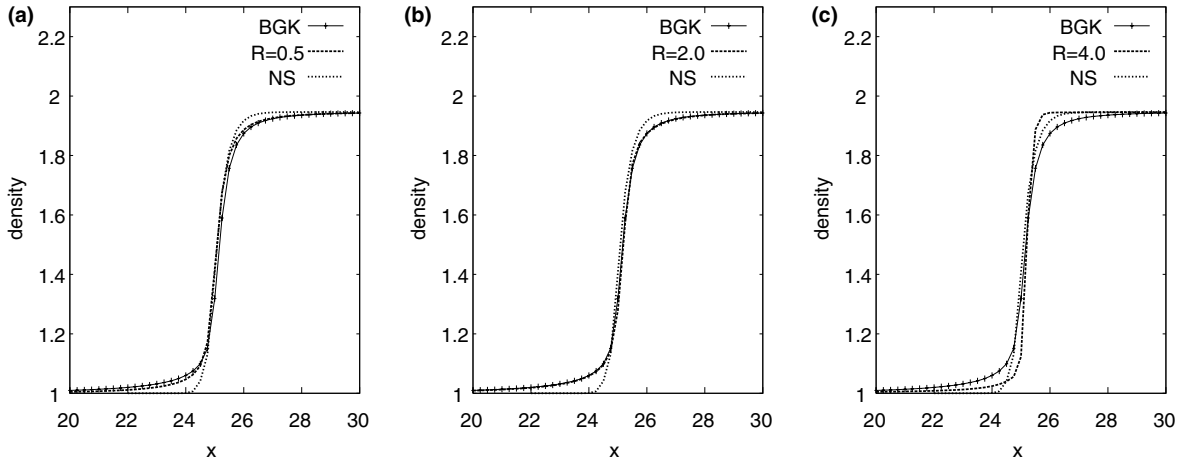


Fig. 1. Stationary shock wave: density as a function of x . The Mach number of the flow is 6. Comparison of the BGK model, the hybrid model and the Navier–Stokes equations for different values of \mathcal{R} ((a) $\mathcal{R} = 0.5$, (b) $\mathcal{R} = 2$, (c) $\mathcal{R} = 4$).

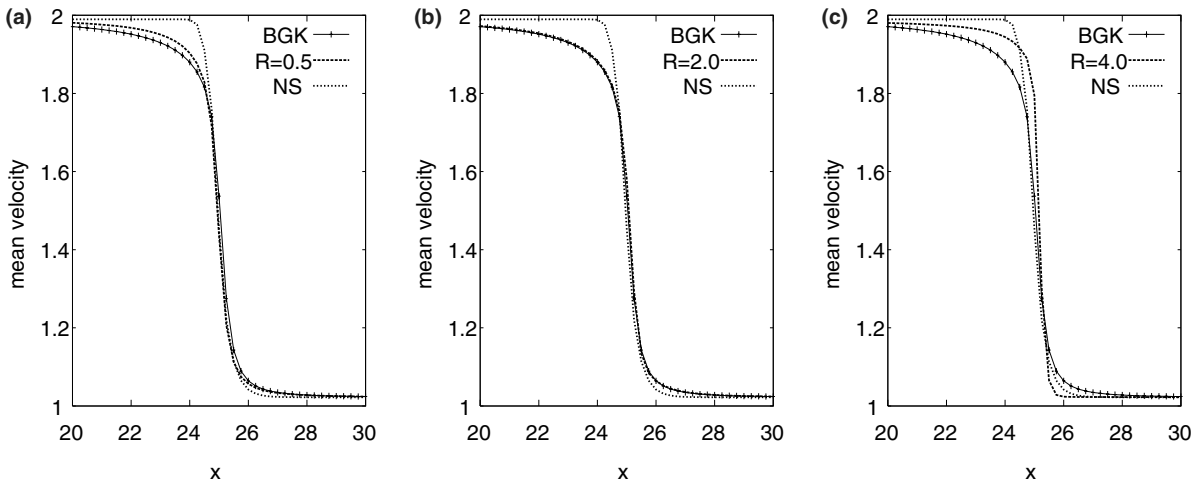


Fig. 2. Stationary shock wave: mean velocity as a function of x . The Mach number of the flow is 6. Comparison of the BGK model, the hybrid model and the Navier–Stokes equations for different values of \mathcal{R} ((a) $\mathcal{R} = 0.5$, (b) $\mathcal{R} = 2$, (c) $\mathcal{R} = 4$).

In Fig. 4, the distribution functions computed by the hybrid model at locations upstream, within, and downstream the shock are plotted as functions of the normalized velocity. On Fig. 5, we compare the distribution function given by the hybrid model to the distribution function given by the full BGK model within the shock, as functions of the velocity variable, for different values of \mathcal{R} . When the flow is at equilibrium, the distribution functions are very well approximated by the hybrid model. On the contrary, inside the shock, our model loses accuracy. Indeed, it reconstructs the distribution function f by a Maxwellian on the ball B_1 whereas f is far from equilibrium in this zone. Nevertheless, the bump in the tail of f is accurately represented by the hybrid reconstruction if \mathcal{R} is sufficiently small. We also notice a small discontinuity at the boundary of the ball: this is the transition between the kinetic unknown f_2 and the Maxwellian \mathcal{M}_1 .

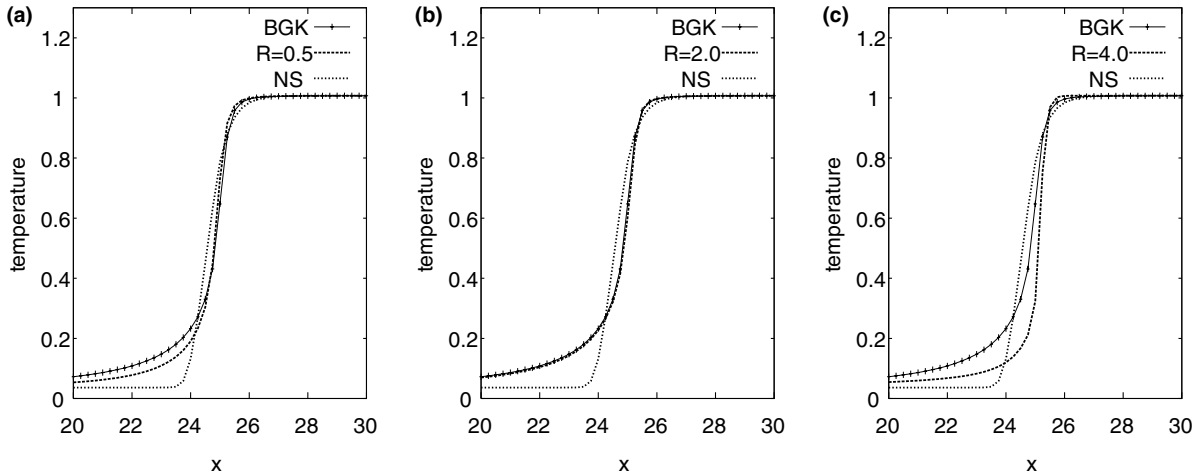


Fig. 3. Stationary shock wave: temperature as a function of x . The Mach number of the flow is 6. Comparison of the BGK model, the hybrid model and the Navier–Stokes equations for different values of \mathcal{R} ((a) $\mathcal{R} = 0.5$, (b) $\mathcal{R} = 2$, (c) $\mathcal{R} = 4$).

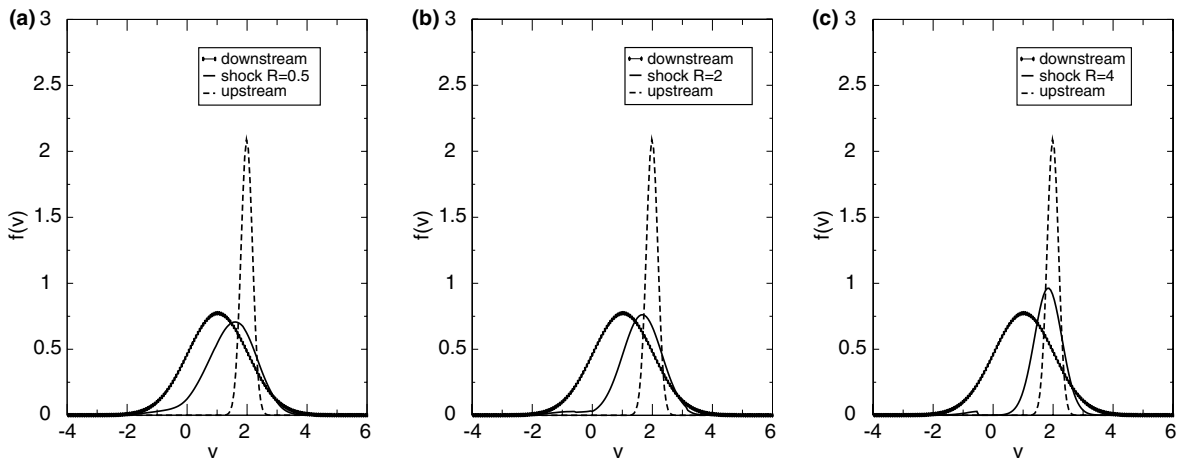


Fig. 4. Stationary shock wave: distribution functions at locations upstream, within and downstream the shock as functions of the normalized velocity, given by the hybrid model for different values of \mathcal{R} ((a) $\mathcal{R} = 0.5$, (b) $\mathcal{R} = 2$, (c) $\mathcal{R} = 4$).

We plot in Fig. 6, the heat flux obtained by the BGK and the hybrid model for different values of \mathcal{R} , as a function of the space. We defined the heat flux by $(1/2) \int_{\mathbb{R}} |v - u|^2 (v - u) f(v) dv$, where u is the mean velocity. It is constant when we are far from the shock and presents very large gradients in the shock zone. The heat flux is accurately described by the hybrid model, since the correct behaviour is reached for sufficiently large \mathcal{R} . Nevertheless, the amplitude of the peak becomes smaller as \mathcal{R} is increasing and a discontinuity is creating downstream the shock ($\mathcal{R} = 4$). In this case, we recover a hydrodynamic behaviour.

4.1.2. Gas dynamics context

In this section, we are interested in the simulation of a rarefied gas flow. As in the previous section, we compare the hybrid model with the associated kinetic model and with the Navier–Stokes equations. The

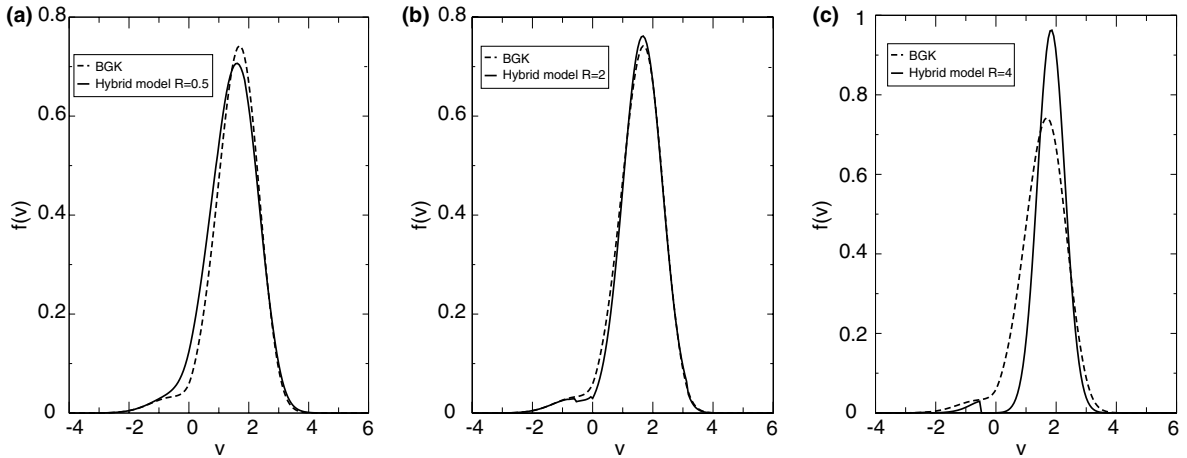


Fig. 5. Stationary shock wave: distribution functions at locations within the shock as functions of the normalized velocity. Comparison of the BGK model and the hybrid model for different values of \mathcal{R} ((a) $\mathcal{R} = 0.5$, (b) $\mathcal{R} = 2$, (c) $\mathcal{R} = 4$).

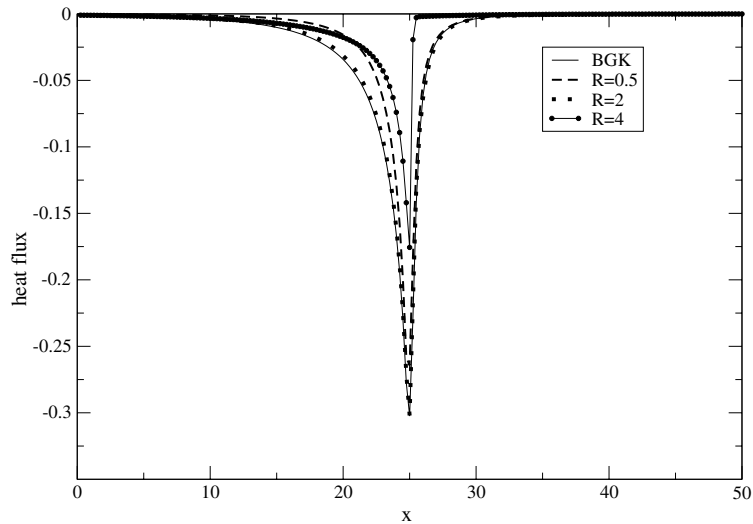


Fig. 6. Stationary shock wave: influence of the parameter \mathcal{R} on the heat flux as a function of x . Comparison of the BGK model and the hybrid model.

basic kinetic model is (4.1), where v is adapted to describe binary collisions between particles in a rarefied gas. Following [38], we choose the collision frequency with a polynomial form in velocity variable

$$v(|v - u|) = \xi |v - u|^\alpha, \tag{4.3}$$

where u is the mean velocity of the flow, $\xi = \xi(t, x)$ and $\alpha > 0$ are determined to reach the correct Prandtl number ($2/3$ for most monoatomic gases). More precisely, an expansion of the solution to the BGK equation (4.1) with the collision frequency (4.3) in power of the Knudsen number ε (Hilbert or Chapman-Enskog expansion [9,10]) can be done. If the second order in ε is retained, both the function $\xi(t, x)$ and

the parameter α can be computed as a function of a reference viscosity coefficient and of the Prandtl number. On the one hand, we find for $\xi(t,x)$

$$\xi(t,x) = \frac{2n}{d(d+2)} \frac{(2RT)^{(2-\alpha)/2}}{\mu} \frac{\Gamma(\frac{4+d-\alpha}{2})}{\Gamma(\frac{d+2}{2})},$$

where $\Gamma(x) = \int_0^{+\infty} t^{x-1} e^{-t} dt$, d is the dimension, n the density and T the temperature, $R = k_B/m$ is the gas constant (k_B denotes the Boltzmann constant and m the particle mass), μ is the viscosity coefficient of the Boltzmann equation: $\mu = \mu_0(T/T_0)^{\alpha/2}$ and μ_0, T_0 are, respectively, the reference viscosity at the temperature T_0 ($\mu_0 = 2.117 \times 10^{-5} \text{ N s m}^{-2}$ and $T_0 = 273 \text{ K}$ for argon (see [3])). On the other hand, the power α is equal to 1.3 in order to reach the correct Prandtl number of $2/3$ in dimension one in the velocity variable. Finally, the collision frequency (4.3) has the following expression:

$$v(|v-u|) = \frac{2n}{3} \frac{(2RT)^{(2-\alpha)/2}}{\mu} \frac{\Gamma(\frac{5-\alpha}{2})}{\Gamma(\frac{3}{2})} |v-u|^\alpha, \quad \alpha = 1.3. \tag{4.4}$$

This collision frequency has already been implemented in [33] for the BGK model.

The shock profiles of the macroscopic quantities (density, mean velocity and temperature) obtained by the BGK model, the Navier–Stokes equations and the hybrid model for different values of \mathcal{R} are presented on Figs. 7–9. As in the plasma context, the hybrid model has an intermediate behaviour between the kinetic model and the hydrodynamic one. When \mathcal{R} is small enough, the hybrid model is very close to the BGK model whereas the profiles become stiffer as \mathcal{R} increases. We observe that the curves obtained by our model with $\mathcal{R} = 2$ are not very correct upstream the shock. Our method suffers of the problem of the discontinuity in the profiles of the macroscopic variables. This phenomenon is characteristic of the classic moment methods (see [22,30]). Large values of \mathcal{R} give very stiff profiles which correspond to profiles given by Euler equations.

We plot in Fig. 10, the distribution functions computed by the hybrid model at locations upstream, within and downstream the shock. In Fig. 11, we compare the results given by the hybrid model to the results of the full BGK model on the distribution function within the shock, as a function of the velocity variable. As in [14], the departure from the equilibrium is not very well described by the hybrid model. The method

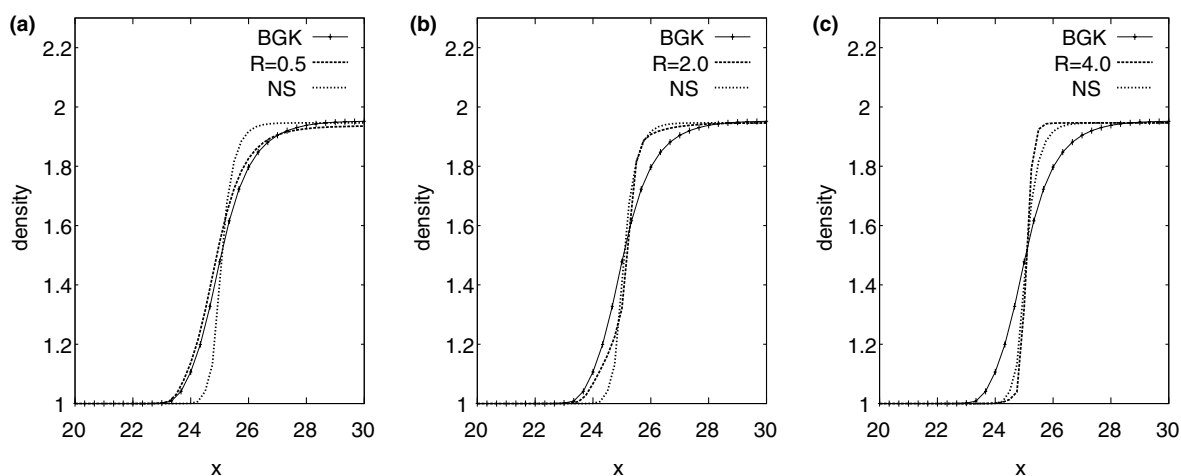


Fig. 7. Stationary shock wave: density as a function of x . The Mach number of the flow is 6. Comparison of the BGK model, the hybrid model and the Navier–Stokes equations for different values of \mathcal{R} ((a) $\mathcal{R} = 0.5$, (b) $\mathcal{R} = 2$, (c) $\mathcal{R} = 4$).

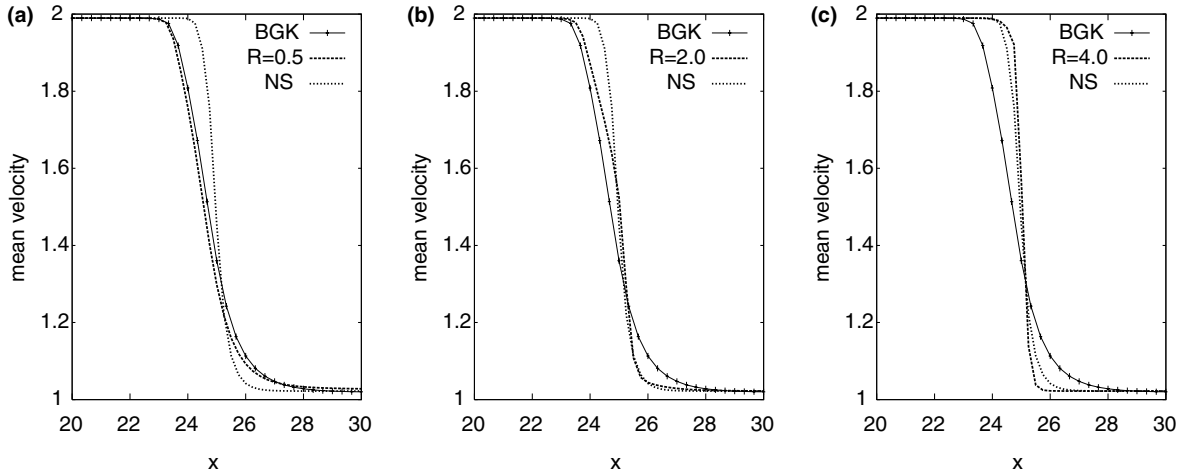


Fig. 8. Stationary shock wave: mean velocity as a function of x . The Mach number of the flow is 6. Comparison of the BGK model, the hybrid model and the Navier–Stokes equations for different values of \mathcal{R} ((a) $\mathcal{R} = 0.5$, (b) $\mathcal{R} = 2$, (c) $\mathcal{R} = 4$).

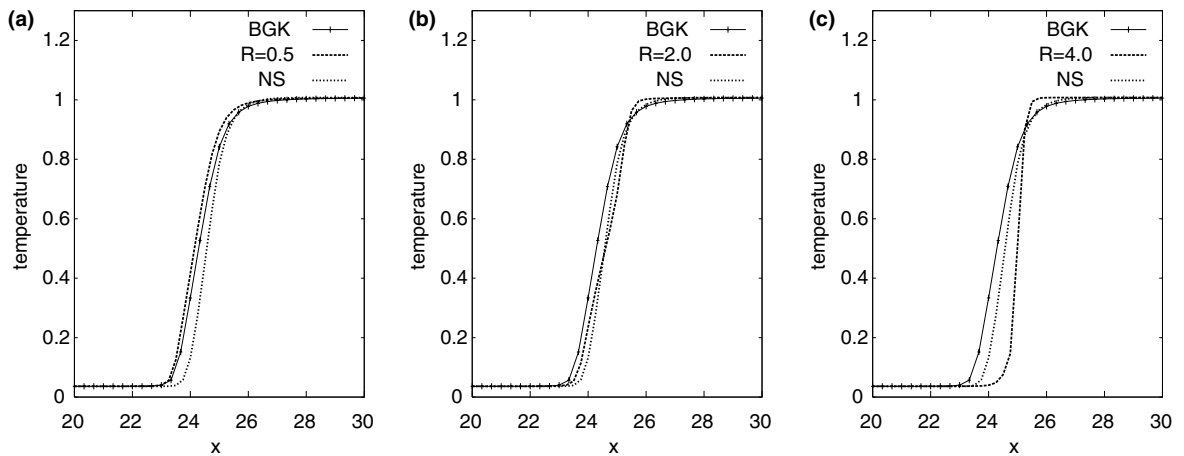


Fig. 9. Stationary shock wave: temperature as a function of x . The Mach number of the flow is 6. Comparison of the BGK model, the hybrid model and the Navier–Stokes equations for different values of \mathcal{R} ((a) $\mathcal{R} = 0.5$, (b) $\mathcal{R} = 2$, (c) $\mathcal{R} = 4$).

needs a very small \mathcal{R} to recover the results given by the kinetic model (e.g., for $\mathcal{R} = 0.5$, the reconstructed distribution function is very close to f). On the contrary, when \mathcal{R} is greater ($\mathcal{R} = 4$), the distribution functions given by the hybrid model become Maxwellians and we recover hydrodynamical results; hence, in these cases, our model is not accurate enough.

Finally, Fig. 12 presents the heat flux approximated by both the kinetic model and the hybrid model for different \mathcal{R} . For the definition of the heat flux, we consider $(1/2)\int_{\mathbb{R}}|v-u|^2(v-u)f(v)dv$, where u denote the mean velocity. The hybrid model gives interesting results; besides, when \mathcal{R} is small enough, we recover the results of the kinetic model, as expected. As \mathcal{R} is growing, the amplitude of the peak becomes small compared to the results obtained by the BGK model.

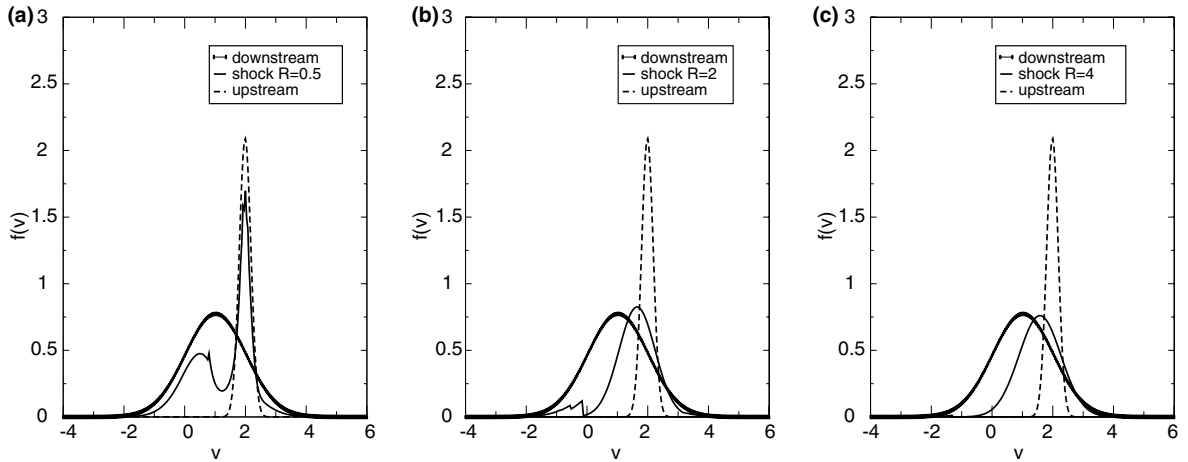


Fig. 10. Stationary shock wave: distribution functions at locations upstream, within and downstream the shock as functions of the normalized velocity, given by the hybrid model for different values of \mathcal{R} ((a) $\mathcal{R} = 0.5$, (b) $\mathcal{R} = 2$, (c) $\mathcal{R} = 4$).

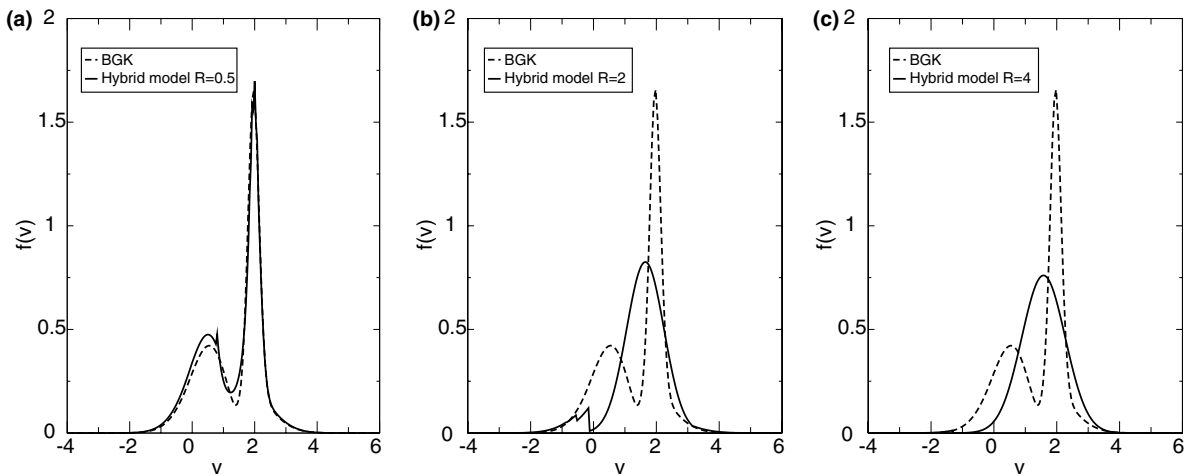


Fig. 11. Stationary shock wave: distribution functions at locations within the shock as functions of the normalized velocity. Comparison of the BGK model and the hybrid model for different values of \mathcal{R} ((a) $\mathcal{R} = 0.5$, (b) $\mathcal{R} = 2$, (c) $\mathcal{R} = 4$).

4.2. Landau damping without collision

In this section, we propose to validate our method against the standard test case of the linear Landau damping. This test is a collisionless one but a self-consistent electric field is considered through the Poisson equation. We study the evolution of electrons whose distribution function is, initially, an isotropic Maxwellian of density n_0 and of temperature T_0 . The plasma is then perturbed and a periodic damped wave is created. The object of this test is the study of the evolution of this damped wave. To that purpose, we consider the distribution function of electrons which is a solution to the Vlasov–Poisson equation

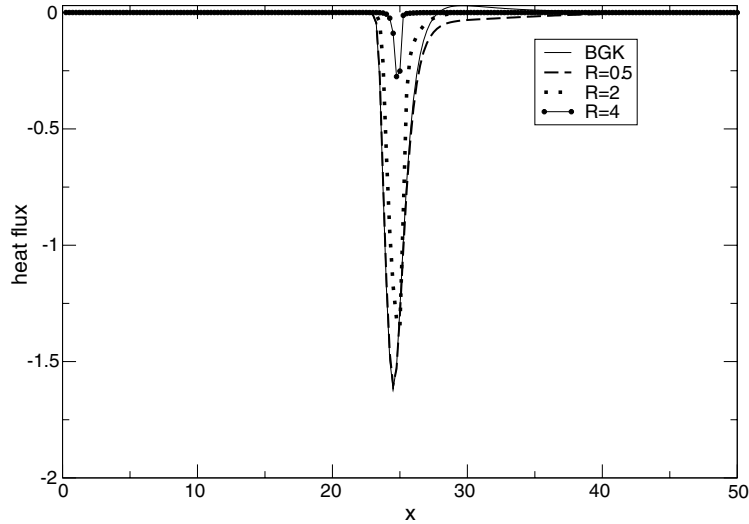


Fig. 12. Stationary shock wave: influence of the parameter \mathcal{R} on the heat flux as a function of x . Comparison of the BGK model and the hybrid model.

$$\frac{\partial f}{\partial t} + v \cdot \nabla_x f + \frac{e}{m_e} E \cdot \nabla_v f = 0,$$

where the self-consistent electric field E is coupled to the Poisson equation

$$\partial_x E = \frac{e}{\epsilon_0} \left(\int_{\mathbb{R}} f(v) \, dv - n_i \right),$$

where e is the unit charge, m_e the electron mass, ϵ_0 the permittivity of free space and n_i the ion density which we assume to be constant. To accurately describe the physical phenomena, we introduce dimensionless parameters. Hence, we introduce the plasma frequency ω_p , the Debye length λ_D and the thermic velocity of electrons v_{th} by:

$$\omega_p = \sqrt{\frac{n_0 e^2}{\epsilon_0 m_e}}, \quad \lambda_D = \sqrt{\frac{\epsilon_0 k_B T_0}{n_0 e^2}}, \quad v_{th} = \sqrt{\frac{k_B T_0}{m_e}}, \tag{4.5}$$

where k_B is the Boltzmann constant. The scaled initial condition associated to the scaled Vlasov–Poisson equation has the following form:

$$f_0(x, v) = \frac{1}{\sqrt{2\pi}} \exp\left(-\frac{v^2}{2}\right) (1 + \alpha \cos(kx)), \quad (x, v) \in [0, 2\pi/k] \times \mathbb{R}, \tag{4.6}$$

where α is the amplitude of the initial wave and k is the scaled wave number. The parameter α is taken small enough such that we only consider linear regimes.

To capture the Landau damping, the size of the velocity domain must be chosen greater than the phase velocity v_ϕ (see [15]). The phase velocity is given by $v_\phi = \omega/k$, where ω is the frequency related to k and approximated by

$$\omega^2 = 1 + 3k^2.$$

Then, we set $v_{\max} = 6$ where the velocity domain extends from $-v_{\max}$ to v_{\max} . We use a number of cells $N_v = 100$ for the velocity domain and $N_x = 200$ in the spatial direction. The boundary condition for the distribution function are periodic in the space variable. Finally, the wave number is fixed to $k = 0.3$ and $\alpha = 0.001$. The same numerical parameters are used for the kinetic model.

In this test, we are interested in the evolution of the square root of the electric energy approximated by

$$\mathcal{E}_h(t) = \left(\sum_i E_i^2(t) \Delta x \right)^{1/2}. \tag{4.7}$$

Indeed, according to the Landau theory, the amplitude of $\mathcal{E}_h(t)$ is expected to be exponentially decreasing with a frequency ω .

In Fig. 13, we plot the evolution of $\mathcal{E}_h(t)$ in logarithmic scale as a function of time, for the Vlasov–Poisson model and for the hybrid model for comparison. We also plot a line (which we call Landau line) which passes through the maximum of each period of (4.7). For small \mathcal{R} and for the Vlasov–Poisson equation, we observe that the amplitude of $\mathcal{E}_h(t)$ is damped exponentially in time as predicted by the Landau theory. On the contrary, as \mathcal{R} is growing, the damping is not exponential any more for the hybrid model. Even if the hybrid model gives a damped wave, the amplitude of $\mathcal{E}_h(t)$ oscillates around the Landau line. For large values of \mathcal{R} , these oscillations are amplified and we observe that they are not damped any more.

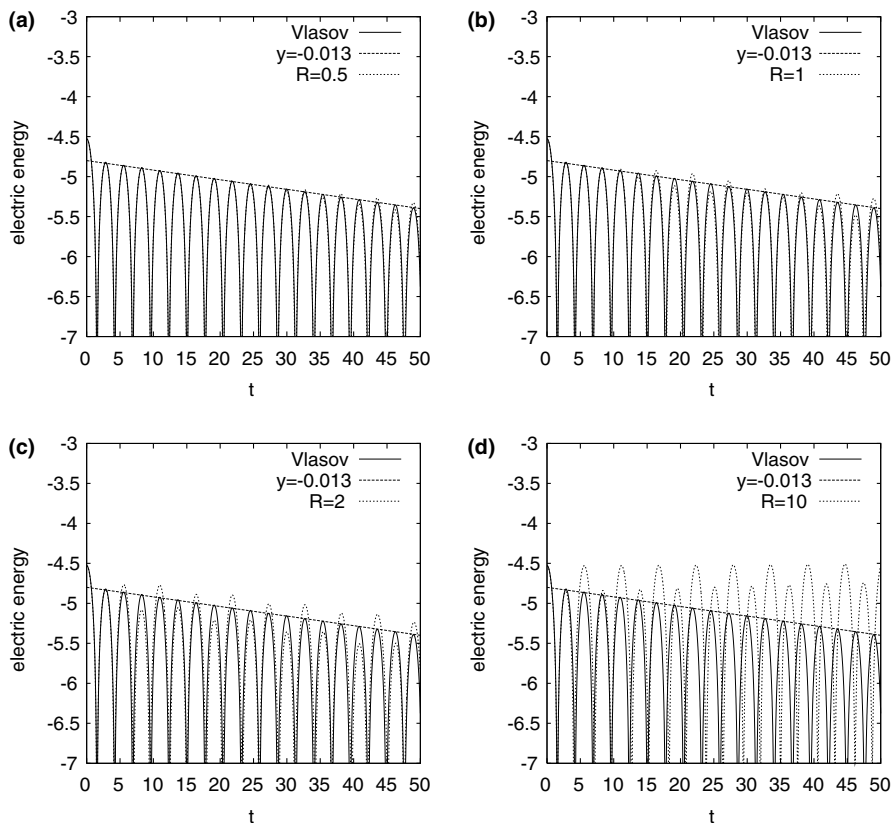


Fig. 13. Linear Landau damping: electric energy as a function of time in log scale. Study of the influence of \mathcal{R} . Comparison of the Vlasov–Poisson model and the hybrid model. $k = 0.3$ and $\alpha = 0.001$.

Thanks to the Landau theory, the numerical results can be compared from a quantitative point of view. Indeed, if we linearize the Vlasov–Poisson system, the damping rate of the amplitude of $\mathcal{E}_h(t)$ can be estimated by solving the dispersion relation [2,11]. However, when k is small enough, a more accurate formula, which is obtained by increasing the order of the Taylor expansion predicts the damping rate of the amplitude of the electric energy (see [25,15]):

$$\gamma = \sqrt{\frac{\pi}{8}} \left(\frac{1}{k^3} - 6k \right) \exp \left(-\frac{1}{2k^2} - \frac{3}{2} - 3k^2 \right). \quad (4.8)$$

Our numerical results are in good agreement with (4.8) for the Vlasov–Poisson system and for the hybrid model for small \mathcal{R} . As \mathcal{R} is growing, the amplitude of $\mathcal{E}_h(t)$ moves away from the Landau line. In Fig. 14, we plot the electric energy (in logarithm scale) as a function of time given by the hybrid model with a large value of \mathcal{R} and by the Euler–Poisson model discretized using a high order WENO method [37]. We observe a wave with two different amplitudes for which the damping is zero. This is explained by the fact that the Landau damping is a purely kinetic effect which cannot be derived from the hydrodynamic theory (see [2,11]). We also notice that the two curves of Fig. 14 become different at large times. One explanation can be the following. The WENO method uses a high order approximation (order 4 in time and order 5 in space) whereas the hybrid model is discretized by means of a first order method.

4.3. Ion acoustic wave

In this section, we study the frequency and damping of ion acoustic waves. This numerical test takes account of both the electric field and collisions. We then consider the Eqs. (1.2) and (1.3) (where v is given by (2.1)) to describe the evolution of the ion acoustic waves in a singly ionized plasma (see [34]). As the ionic mean free path is bigger than the electron one, we can consider a constant electron temperature; in this case, the electric field satisfies

$$\frac{eE}{m} = -\frac{k_B}{m} T_e \frac{\nabla_x n}{n},$$

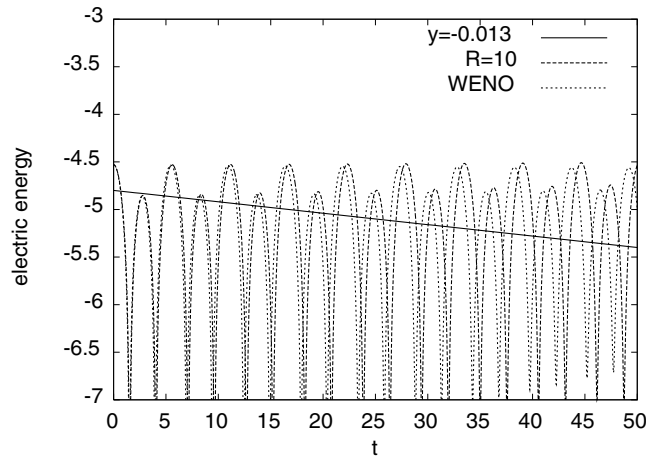


Fig. 14. Linear Landau damping: electric energy as a function of time in log scale. Comparison of the hybrid model and the Euler–Poisson model. $k = 0.3$ and $\alpha = 0.001$.

where m is the ionic mass, k_B the Boltzmann constant, T_e is the electronic temperature, and n denotes the ionic density (see [34]). The starting kinetic equation then reads

$$\frac{\partial f}{\partial t} + v \cdot \nabla_x f - \frac{k_B T_e}{mn} \nabla_x n \cdot \nabla_v f = \nu(\mathcal{M}_{[f,\nu]} - f), \tag{4.9}$$

where $\nu = \nu(t,x,v)$ is the collision frequency given by (2.1).

By choosing an initial condition of the form of (4.6), the density and the mean velocity have a purely exponential behaviour, i.e., $\exp(i\omega t + \gamma t)$. The damping γ and the frequency ω represent the solution of the dispersion relation. Thus, by changing k , the desired functions $\omega(k)$ and $\gamma(k)$ are determined.

As in [34], we rescale (4.9) using the ionic mean free path $l = (k_B T_i)^2 / (4\pi n_0 e^4 \ln \Lambda)$, (with T_i the ionic temperature, n_0 the unperturbed density, e the charge and $\ln \Lambda$ the Coulombian logarithm) as unit of length, $v_0 = (k_B T_i / m)^{1/2}$ as unit of velocity and the collisional ion–ion time $\tau = llv_0$ as unit of time. Consequently, in these units, (4.9) is written

$$\frac{\partial f}{\partial t} + v \cdot \nabla_x f - \frac{T_e}{T_i} \frac{\nabla_x n}{n} \cdot \nabla_v f = \nu(\mathcal{M}_{[f,\nu]} - f). \tag{4.10}$$

We consider a rescaled initial condition of the form

$$f_0(x, v) = \frac{n_0}{(2\pi)^{1/2}} \exp\left(-\frac{|v|^2}{2}\right) (1 + \alpha \cos(kx)), \quad (x, v) \in [0, 2\pi/k] \times \mathbb{R}, \tag{4.11}$$

where k is the wave number and α is the perturbation (α is chosen small enough to consider linear regimes). Note that n_0 can be taken equal to 1 because the problem is homogeneous in f . The only dimensionless parameter of the problem are the ratio T_e/T_i and k ; as proposed in [34], we will consider different ratios of temperature (equal to 1, 2, 4) with different k (from 0.025 to 1).

To accurately describe the physics of the test, we consider a velocity set from $-v_{\max}$ to v_{\max} with $v_{\max} = 6$. We use a number of cells $N_v = 50$ in velocity whereas we consider $N_x = 200$ in physical space. Besides, the perturbation α is equal to 0.001. The same numerical parameters are used for the kinetic model.

In Figs. 15–17, we plot the quantity γ/k (where γ is the damping rate of the perturbed density and k the wave number) as a function of k . The results obtained by both the Vlasov–BGK equation and the hybrid

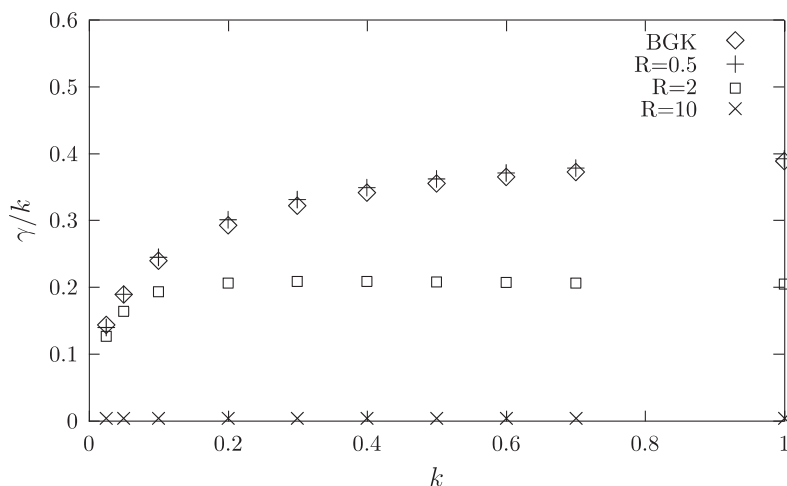


Fig. 15. Ion acoustic waves: γ/k as a function of k for $T_e/T_i = 4$. Comparison between the BGK model and the hybrid model.

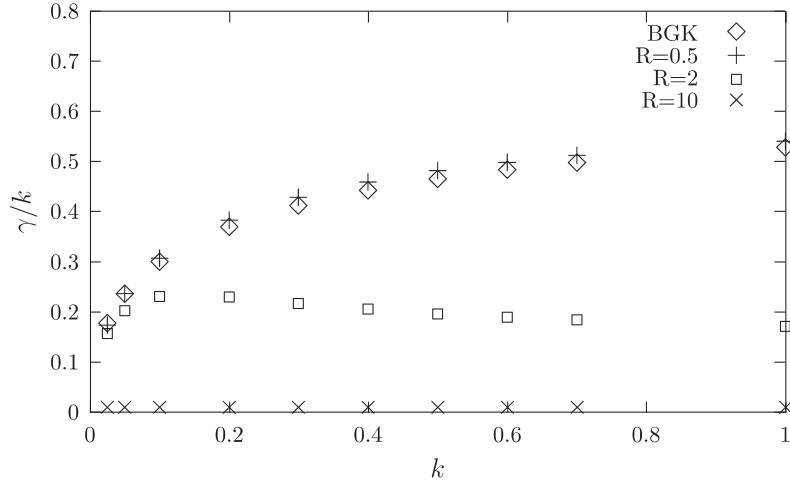


Fig. 16. Ion acoustic waves: γ/k as a function of k for $T_e/T_i = 2$. Comparison between the BGK model and the hybrid model.

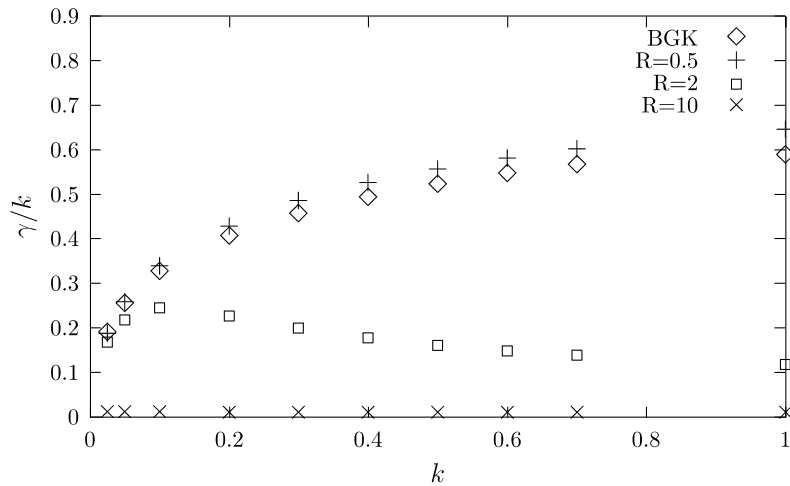


Fig. 17. Ion acoustic waves: γ/k as a function of k for $T_e/T_i = 1$. Comparison between the BGK model and the hybrid model.

model (for various \mathcal{R}) are presented. When $\mathcal{R} = 0.5$, the hybrid model gives satisfying results since they are very close to the full kinetic one. When $\mathcal{R} = 2$, the results are in correct agreement with the BGK ones for small values of k . As k increases, γ/k moves away from the kinetic results and decreases. Besides, as \mathcal{R} is growing, the results become far from that obtained by the kinetic model. For example, the value $\mathcal{R} = 10$ (which corresponds to a full hydrodynamic model) gives a very small damping ($\gamma \approx 0$). Like in Landau damping case, hydrodynamic models cannot reach the ion acoustic wave damping.

We also compare our results to [34]. From a qualitative point of view, both the BGK model and the hybrid model for $\mathcal{R} = 0.5$ are in good agreement with [34]. In particular, we observe that the behaviour of γ/k is proportional to k when we consider small values of k ($k < 0.2$). Besides, for larger values of k , γ/k becomes nearly constant and is more important when the ratio T_e/T_i decreases. From a quantitative point of view, even if our numerical results do not coincide exactly with [34], they are in correct agreement.

Indeed, at the collisional and collisionless limits (i.e., $k = 0$ and $k = +\infty$), our results are close to the predicted values of ω/k (obtained by linearizing (4.9)). The differences between our results and those of [34] can be explained in two ways. First, in [34], the authors consider the whole 3 dimensional case in the velocity variable and second, they solve the linearized Fokker–Planck–Landau problem whereas a simpler collision operator of BGK type is used here.

In Figs. 18–20, we plot ω/k as a function of k . The same remarks made previously hold. Indeed, the behaviour of the curves is correct for both the BGK model and the hybrid model for small \mathcal{R} , since, for small k , we recover the approximation obtained by the linearization

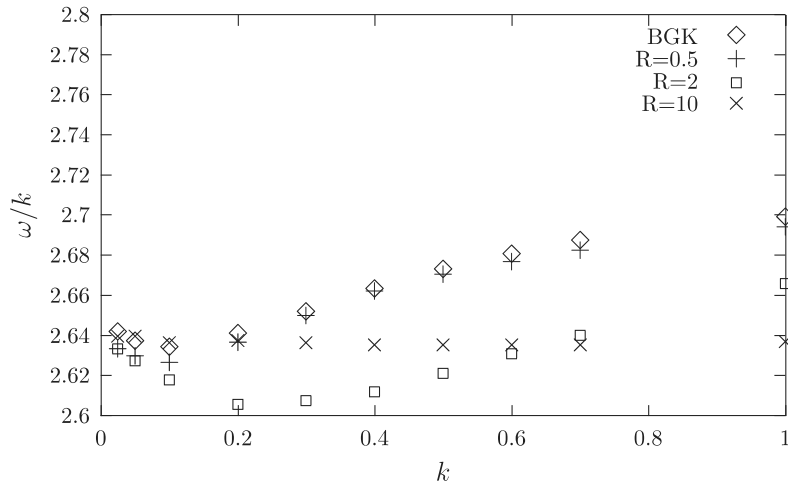


Fig. 18. Ion acoustic waves: ω/k as a function of k for $T_e/T_i = 4$. Comparison between the BGK model and the hybrid model.

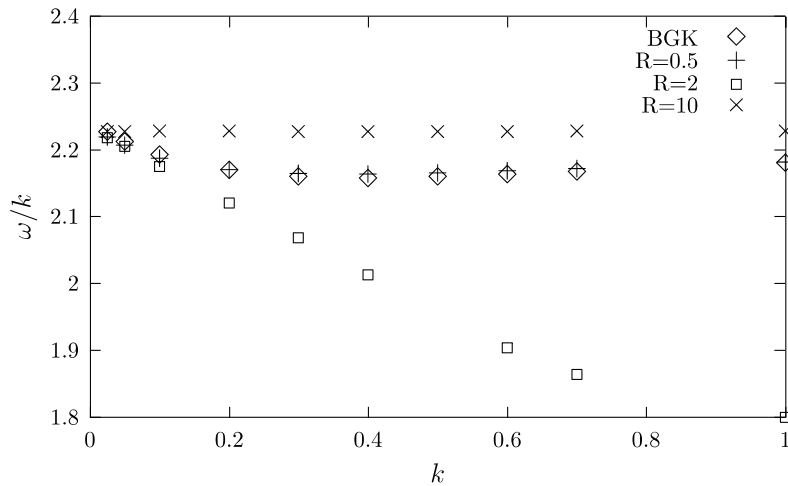


Fig. 19. Ion acoustic waves: ω/k as a function of k for $T_e/T_i = 2$. Comparison between the BGK model and the hybrid model.

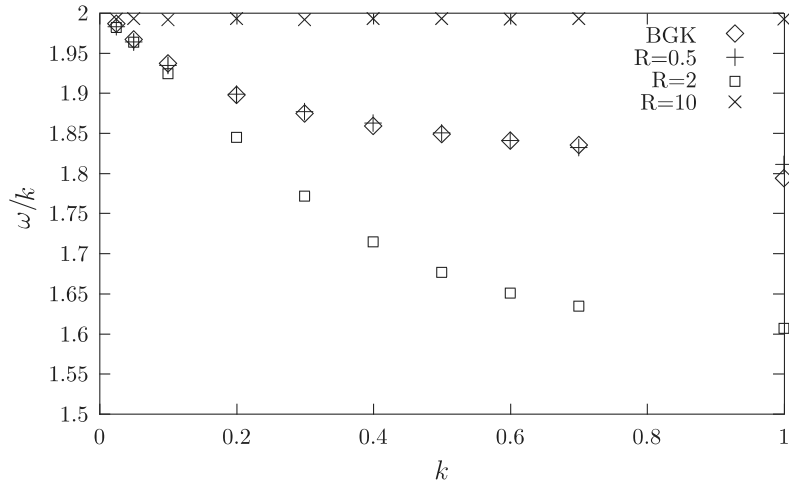


Fig. 20. Ion acoustic waves: ω/k as a function of k for $T_e/T_i = 1$. Comparison between the BGK model and the hybrid model.

$$\omega^2 = \left(3 + \frac{T_e}{T_i} \right).$$

Besides, we observe that, at the beginning, ω/k slowly decreases as k increases. After some time, according to the considered ratio, ω/k increases slowly or remains almost constant. A similar behaviour has also been noticed in [34]. However, when \mathcal{R} is bigger, the numerical results given by the hybrid model are not correct. Indeed, we observe that for $\mathcal{R} = 2$, ω/k is a decreasing function of k , and for $\mathcal{R} = 10$, ω/k remains almost constant. Thus, in this case, the numerical results are not in good agreement with estimated values.

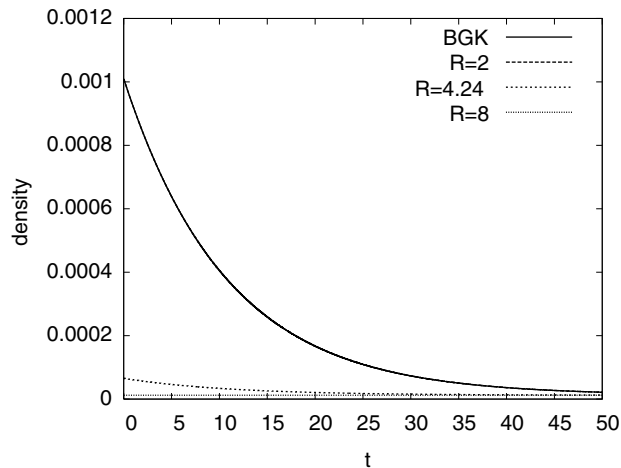


Fig. 21. Electron beam: density of the beam as a function of time. Comparison between the BGK model and the hybrid model.

4.4. Electron beam

In this section, we propose to validate our hybrid model by modelling the deceleration of an electron beam in a plasma. Let us consider a beam of electrons that enter in a plasma composed of electrons. We consider the plasma at equilibrium. Let us denote by $f = f(t, x, v)$ the density of the electrons in the phase space (x, v) . The evolution of f can be modeled by the following scaled kinetic equation:

$$\frac{\partial f}{\partial t} + v \cdot \nabla_x f = \nu(\mathcal{M}_{[f,v]} - f), \tag{4.12}$$

where ν is given by (2.1). Eq. (4.12) is supplemented with the following initial condition:

$$f_0(x, v) = \mathcal{M}_{n_e, u_e, T_e} + \mathcal{M}_{n_b, u_b, T_b},$$

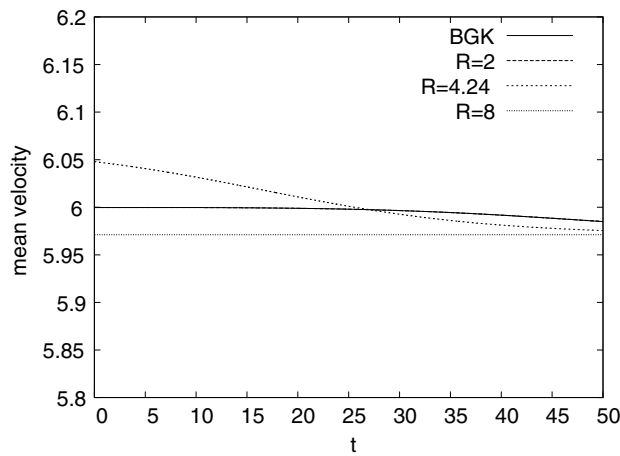


Fig. 22. Electron beam: mean velocity of the beam as a function of time. Comparison between the BGK model and the hybrid model.

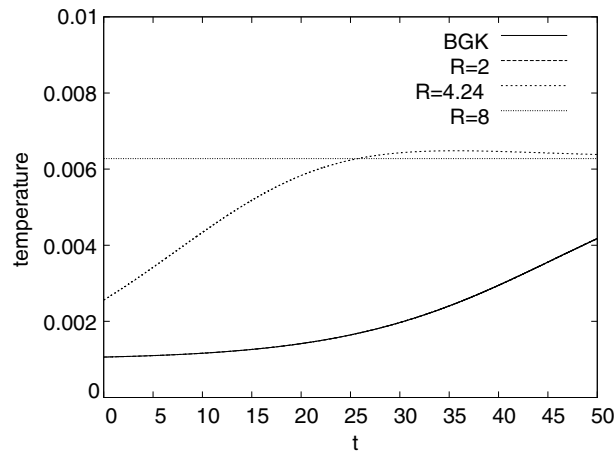


Fig. 23. Electron beam: temperature of the beam as a function of time. Comparison between the BGK model and the hybrid model.

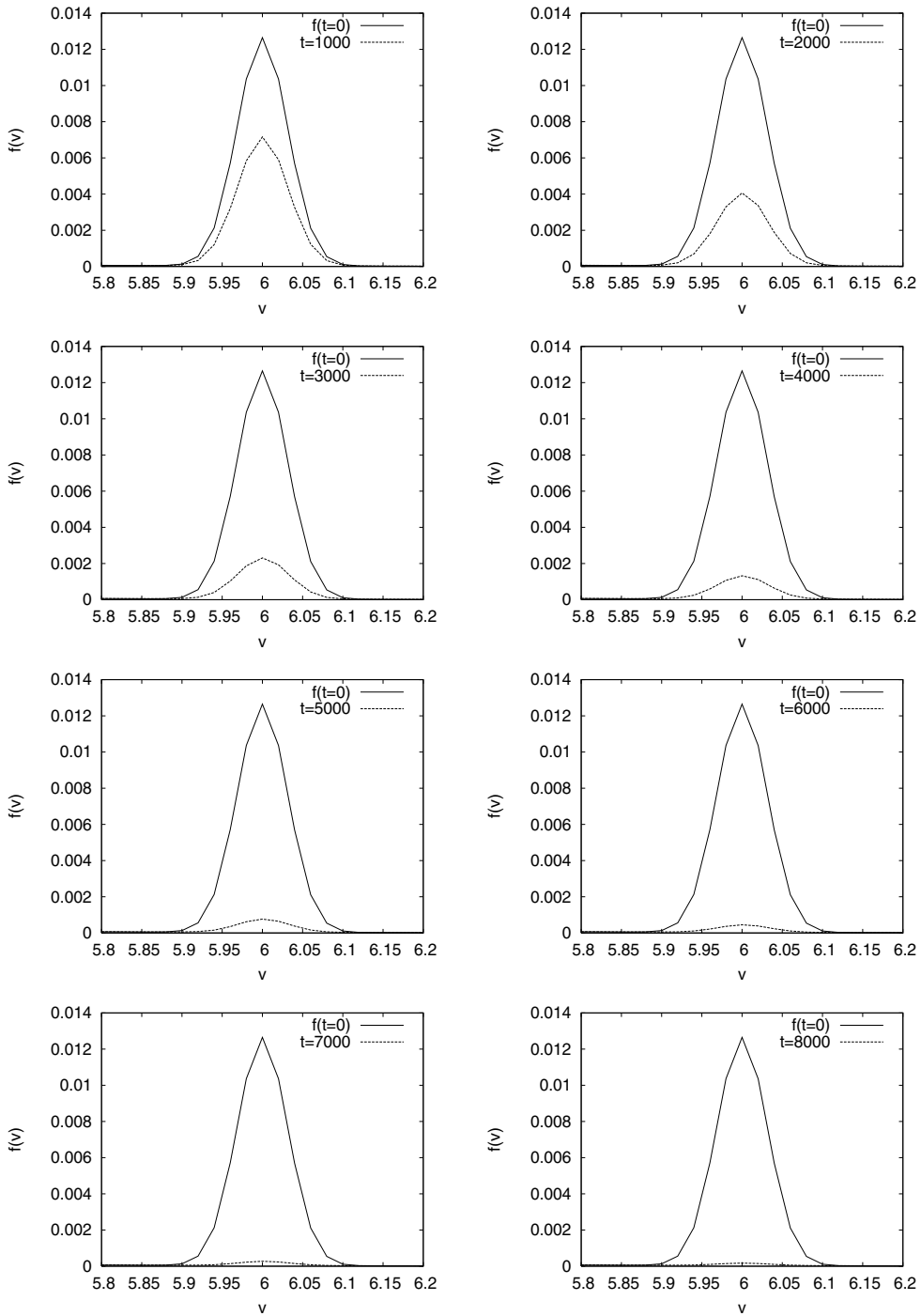


Fig. 24. Evolution of the beam: distribution function as a function of the velocity.

where $\mathcal{M}_{n,u,T} = n/\sqrt{2\pi T} \exp(-|v-u|^2/(2T))$, n_e, u_e, T_e are the plasma parameters and n_b, u_b, T_b the parameters of the beam. In this test, we choose $n_e = 1, u_e = 0, T_e = 2$ for the parameters of the plasma and $n_b = 0.001, u_b = 6, T_b = 0.001$ are the beam parameters.

The velocity set extends from $-v_{\max}$ to $v_{\max} = 8$ whereas the space domain is equal to $[0,1]$. We consider $N_v = 400$ cells in velocity because the beam temperature is low whereas $N_x = 50$ is used to discretize the physical space. Some periodic conditions are implemented in space whereas the distribution function is truncated for large velocities. The same numerical parameters are used for the kinetic model.

We are interested in the evolution in time of the density, mean velocity and temperature of the beam. As explained in [26], the electron beam is decelerated by collisions with the particles of the plasma (electrons in our case).

In Figs. 21–23, we plot the evolution in time of the density, mean velocity and temperature of the beam. We observe that the density is decreasing in time. Moreover, the mean velocity remains constant equal to the initial mean velocity of the beam. We also notice that the temperature is almost constant at the beginning before increasing strongly. We remark that the results obtained by the hybrid model with $\mathcal{R} \leq 4$ are superposed on the kinetic results. Indeed, the evolution of the beam is then described by the kinetic part of the hybrid model.

In Fig. 24, we study the evolution in time of the beam by plotting the distribution function as a function of the velocity v . We observe that the density of the beam decreases whereas its mean velocity remains constant. As remarked above, the hybrid model gives the same results as the kinetic one when the radius of B_1 is smaller than u_b . Indeed, in this case, the beam is situated in the kinetic part of the hybrid model. On the contrary, when \mathcal{R} is sufficiently large, i.e., the beam is contained in B_1 , nothing happens. The density, mean velocity and temperature remains constant. An intermediate behaviour occurs when the beam is treated by both the fluid and the kinetic equations ($\mathcal{R} = 4.24$). Nevertheless, the results given the hybrid model in such a case are not correct. Indeed, the use of a fluid model to treat the beam is not accurate at all. In this case, we notice that the numerical results are very far from the results given by the full kinetic model.

This test case shows the limitation of a BGK collision operator. Indeed, whereas the full Fokker–Planck–Landau operator decelerates the beam (its mean velocity decreases), the BGK operator takes particles off the beam into the plasma without changing the mean velocity of the beam. Hence, the mean velocity remains constant, which is not correct from a physical point of view.

Remark 4.1. Even if in the present stage of our work the numerical cost does not depend on \mathcal{R} , an a priori determination of a suitable \mathcal{R} can be important. Such a choice can be made in some particular cases (stationary shock wave for instance), but remains difficult in the general case. However, note that the parameter \mathcal{R} may depend on time and on space, but also on the Knudsen number. For instance, in the test case of the stationary shock wave, \mathcal{R} can be small at locations where the flow is known to be far from equilibrium without destroying the accuracy. An x -dependent \mathcal{R} can then be used. Applications concerning nonlinear Landau damping can also be considered since after a long time, the solution becomes close to a Maxwellian with some particles trapped in the tail. In this last case, a time-dependent \mathcal{R} would be appropriate.

5. Conclusion

We have presented an extension of the hybrid model introduced in [13,14] to describe systems of charged particles. This model is derived using a domain-decomposition in the velocity space and an approximation of the solution to the kinetic equation is made for small velocities. This approximation is based on a mo-

ment method with an entropy minimization principle. The starting kinetic model is a Vlasov–BGK-like equation. It takes account of an electric field and a velocity-depending collision frequency computed from the Fokker–Planck–Landau collision operator.

Then, various numerical simulations have been made to validate the obtained hybrid model. Comparisons between the BGK model, the Navier–Stokes equations and the hybrid model are presented.

The hybrid model is a compromise between a kinetic and a fluid regimes and, by varying \mathcal{R} , we can cross between the pure fluid to the full kinetic solution. The parameter \mathcal{R} is a kind of cutover between Maxwellian and kinetic solvers.

Consequently, the present approach could be used to correctly describe some systems of particles with a reduced cost compared to a pure kinetic description. However, this reduction has not been the main subject of this work and the hybrid model is as costly as a direct implementation of a kinetic model. All we have done is the derivation and the numerical validation of the hybrid model. Nevertheless, the optimization procedure can be done in several ways: a pre-storage of the numerical fluxes, an explicit computation of the fluxes, the rapid calculation of the Maxwellian parameters in terms of its moments on a ball and, finally, the use of a particle method for the kinetic part. This task is under investigations.

From the hybrid model, one can derive a bi-fluid model in which the kinetic part is also approximated by a fluid model. The bi-fluid model is another intermediate model between the kinetic and the fluid description. Besides, collisions between different species of particles (e.g. electrons and ions) can also be taken into account. Future work will be dedicated to the two latter points.

Acknowledgements

Support by the Commissariat à l'énergie atomique (LRC MIP-CEA M06) and by the European network HYKE (EC contract HPRN-CT-2002-00282), is acknowledged. The authors thank B. Dubroca, J.P. Morreuw and V.T. Tickonchuk for stimulating discussions and encouragements.

Appendix A. Computation of a collision frequency

This section is devoted to the computation of the collision frequency (2.1). Our starting point is the bilinear FPL operator

$$Q(f, g) = C_{\text{FP}} \nabla_v \cdot \int_{\mathbb{R}^3} \Phi(v-w) (g(w) \nabla_v f(v) - \nabla_w g(w) f(v)) dw, \quad (\text{A.1})$$

where $C_{\text{FP}} = e^4 \ln \Lambda / (8\pi m^2 \varepsilon_0^2)$ (e is the electric charge, $\ln \Lambda$ is the usual Coulomb logarithm and ε_0 is the permittivity of free space), m is the mass of the considered particles and $\Phi(v)$ is the 3×3 matrix

$$\Phi(v) = \left(I_3 - \frac{v \otimes v}{|v|^2} \right) \frac{1}{|v|}$$

with I_3 the identity matrix. This operator describes the interactions between electrons. The distribution function of test particles is f whereas g denotes the distribution function of a background. Let us consider that the particles of the background are at the local equilibrium, i.e., their associated distribution function is a Maxwellian M whose parameters are n , u , T . Then, (A.1) becomes

$$Q(f, M) = C_{FP} \nabla_v \cdot \left[(\nabla_v f(v)) \int_{\mathbb{R}^3} \Phi(v-w) M(w) \, dw \right] - C_{FP} \nabla_v \cdot \left[f(v) \int_{\mathbb{R}^3} \Phi(v-w) \nabla_w M(w) \, dw \right], \tag{A.2}$$

where $M(v)$ denotes the Maxwellian of parameters n the density, u the mean velocity and T the temperature

$$M(v) = \frac{n}{(2\pi RT)^{3/2}} \exp\left(-\frac{|v-u|^2}{2RT}\right)$$

and $R = k_B/m$ with k_B the Boltzmann constant, is the constant gas. The collision frequency of the FPL collision operator is obtained using the loss term of (A.2)

$$v(v-u)(v-u) := -C_{FP} \int_{\mathbb{R}^3} \Phi(v-w) \nabla_w M(w) \, dw. \tag{A.3}$$

So, we have to compute the following quantity:

$$v(v-u)(v-u) = C_{FP} \frac{n}{(2\pi RT)^{3/2}} \frac{1}{RT} \int_{\mathbb{R}^3} \Phi(v-w) \exp\left(-\frac{|w-u|^2}{2RT}\right) \, dw (v-u), \tag{A.4}$$

because the kernel of the matrix $\Phi(v)$ is generated by v . By the following change of variables $w = \sqrt{RT}s + u$ in the integral, we get

$$v(v-u)(v-u) = C_{FP} \frac{n}{(2\pi RT)^{3/2}} \int_{\mathbb{R}^3} \Phi(v-u-s) e^{-|s|^2/2} \, ds (v-u). \tag{A.5}$$

Thanks to a result of [19], the following matrix which depends on v :

$$\int_{\mathbb{R}^3} \Phi(v-s) \exp\left(-\frac{|s|^2}{2}\right) \, ds$$

has an eigenvalue $\lambda(|v|)$ associated with the eigenvector v

$$\lambda(|v|) = \int_{\mathbb{R}^3} \left(1 - \frac{(v,s)^2}{|v|^2 |s|^2}\right) \frac{1}{|s|} \exp\left(-\frac{|v-s|^2}{2}\right) \, ds.$$

Thanks to this expression, we can compute the behaviour of λ at $|v| = 0$ and at $|v| \rightarrow +\infty$. As $|v|$ goes to zero, we obtain the following limit:

$$\lim_{|v| \rightarrow 0} \lambda(|v|) = \frac{8}{3} \pi.$$

Now, let us compute the behaviour when $|v| \rightarrow +\infty$

$$\lambda(|v|) \sim 2(2\pi)^{3/2} |v|^{-3}. \tag{A.6}$$

Then, we conclude on the behaviour of our collision frequency as $|v-u|$ goes to zero

$$\lim_{|v-u| \rightarrow 0} v(v-u) = \frac{4C_{FP}}{3} (2\pi)^{-1/2} n / (RT)^{3/2} \tag{A.7}$$

and on the behaviour of our collision frequency as $|v-u|$ goes to $+\infty$

$$v(v-u) \sim 2nC_{FP} / |v-u|^3. \tag{A.8}$$

We have obtained the behaviour of our collision frequency at 0 and at $+\infty$. Then, a possible collision frequency can be the following:

$$v(|v-u|) = C_{\text{FP}} \begin{cases} 4/3(2\pi)^{-1/2}n(RT)^{-3/2} & \text{if } |v-u| < C_0\sqrt{RT}, \\ 2n/|v-u|^3 & \text{if } |v-u| > C_0\sqrt{RT}, \end{cases} \quad (\text{A.9})$$

where C_0 is chosen such that $v(|v-u|)$ is a continuous function of $|v-u|$

$$C_0 = \left(\frac{3}{2}\right)^{1/3}(2\pi)^{1/6}.$$

Some similar computations leads to a BGK type collision operator taking into account collisions between different species of particles as electrons and ions.

References

- [1] O. Batishchev, M. Shoucri, A. Batishcheva, I. Shkarofsky, Fully kinetic simulation of coupled plasma and neutral particles in scrape-off layer plasmas of fusion devices, *J. Plasma Phys.* 61 (1999) 347–364.
- [2] A. Bers, J.L. Delcroix, *Physique des plasmas, Savoir Actuel*, Inter Editions CNRS Editions, Paris, 1994.
- [3] G.A. Bird, *Molecular Gas Dynamics and The Direct Simulation of Gas Flows*, Oxford Science Publications, Oxford, 1994.
- [4] C.K. Birdsall, A.B. Langdon, *Plasma Physics via Computer Simulation*, Institute of Physics Publishing, Bristol and Philadelphia, 1991.
- [5] J.F. Bourgat, P. Le Tallec, B. Perthame, Y. Qiu, Coupling Boltzmann and Euler equations without overlapping, domain decomposition methods in science and engineering, *Am. Math. Soc.* (1992) 377–398.
- [6] J.U. Brackbill, P. Kloucek, F.R. Toffoletto, J. Wightman, Coupling of fluid and kinetic models in a one-dimensional domain, in: Poster Presented at the ICPP Conference and the GEM Conference, 2002.
- [7] S. Brunner, E. Valeo, J.A. Krommes, Linear delta- f simulations of nonlocal electron heat transport, *Phys. Plasmas* 7 (7) (2000).
- [8] C. Buet, S. Cordier, P. Degond, M. Lemou, Fast algorithms for numerical, conservative, and entropy approximations of the Fokker–Planck–Landau equation, *J. Comput. Phys.* 133 (1997) 310–322.
- [9] C. Cercignani, *The Boltzmann Equation and Its Applications Lectures Series in Mathematics*, vol. 68, Springer-Verlag, Berlin, 1988.
- [10] S. Chapman, T.G. Cowling, *The Mathematical Theory of Non-uniform Gases*, Oxford University Press, Oxford, 1970.
- [11] F.F. Chen, *Introduction to Plasma Physics and Controlled Fusion*, second ed., Plenum Press, New York and London, 1983.
- [12] N. Crouseilles, Dérivation de modèles couplés dérive-diffusion/cinétique par une méthode de décomposition en vitesse, *CR Acad. Sci. Paris, Ser. I* 334 (2002) 827–832.
- [13] N. Crouseilles, P. Degond, M. Lemou, Hybrid fluid/kinetic models for nonequilibrium systems, *CR Acad. Sci. Paris, Ser. I* 336 (2003) 359–364.
- [14] N. Crouseilles, P. Degond, M. Lemou, A hybrid kinetic–fluid model for solving the gas dynamics Boltzmann–BGK equation, *J. Comput. Phys.* 199 (2004) 776–808.
- [15] N. Crouseilles, F. Filbet, Numerical approximation of collisional plasma by high order methods, *J. Comput. Phys.* 201 (2004) 546–572.
- [16] P. Degond, P.F. Peyrard, G. Russo, P. Villedieu, Polynomial upwind schemes for hyperbolic systems, *CR Acad. Sci. Paris, Ser. I* 328 (1999) 479–483.
- [17] P. Degond, C. Schmeiser, Kinetic boundary layers and fluid–kinetic coupling in semiconductors, *Transp. Theory Stat. Phys.* 28 (1999) 31–55.
- [18] P. Degond, S. Jin, A smooth transition model between kinetic and diffusion equations, preprint MIP, 2003.
- [19] P. Degond, M. Lemou, Dispersion relations for the linearized Fokker–Planck equation, *Arch. Rational Mech. Anal.* 138 (1997) 137–167.
- [20] S. Dellacherie, Contribution à l’analyse et à la simulation numériques des équations cinétiques décrivant un plasma chaud, Ph.D. Thesis, 1998.
- [21] L. Desvillettes, On asymptotics of the Boltzmann equation when the collisions become grazing, *Transp. Theory Stat. Phys.* 21 (1992) 259–276.
- [22] B. Dubroca, A. Klar, Prise en compte d’un fort déséquilibre cinétique par un modèle aux demi-moments, *CR Acad. Sci. Paris, Ser. I* 335 (2002) 699–704.
- [23] F. Filbet, Convergence of a finite volume scheme for the one-dimensional Vlasov–Poisson system, *SIAM J. Numer. Anal.* 39 (2001) 1146–1169.

- [24] F. Filbet, E. Sonnendrucker, P. Bertrand, Conservative numerical schemes for the Vlasov equation, *J. Comput. Phys.* 172 (2001) 166–187.
- [25] C.J. McKinstrie, R.E. Giacone, E.A. Startsev, Accurate formulas for the Landau damping rates of electrostatic waves, *Phys. Plasmas* 6 (2) (1999) 463–466.
- [26] N.A. Krall, A.W. Trivelpiece, *Principles of Plasma Physics*, McGraw-Hill, New York, 1973.
- [27] P. Le Tallec, F. Mallinger, Coupling Boltzmann and Navier–Stokes equations by half fluxes, *J. Comput. Phys.* 136 (1997) 51–67.
- [28] P. Le Tallec, J.P. Perlat, Coupling kinetic models with Navier–Stokes equations, *CFD Rev.* 2 (1998) 833–855.
- [29] C.D. Levermore, Moment closure hierarchies for kinetic theories, *J. Stat. Phys.* 83 (1996) 1021–1065.
- [30] C.D. Levermore, W.J. Morokoff, The Gaussian moment closure for gas dynamics, *SIAM J. Appl. Math.* 59 (1999) 72–96.
- [31] M.L. Marconi, L. Dagum, W.H. Smyth, Hybrid fluid/kinetic-theory approach to modeling atmospheres: the case of an intermediate mass body, *Astrophys. J.* 469 (1996) 393–401.
- [32] L. Mieussens, Discrete velocities model and implicit scheme for the BGK equation of rarefied gas dynamics, *Math. Model Meth. Appl. Sci.* 8 (2002) 1121–1149.
- [33] L. Mieussens, H. Struchtrup, Numerical solution to the BGK model with velocity dependant collision frequency, in: *Symposium on Rarefied Gas Dynamics 23*, AIP Conference Proceedings, vol. 663, 2003, pp. 320–327.
- [34] M. Ono, R.M. Kulsrud, Frequency and damping of ion acoustic waves, *Phys. Fluid* 18 (10) (1975) 88–97.
- [35] S.E. Parker, W.W. Lee, A fully nonlinear characteristic method for gyrokinetic simulation, *Phys. Fluid B* (5) (1993) 77–86.
- [36] M. Shoucri, G. Knorr, Numerical integration of the Vlasov equation, *J. Comput. Phys.* 14 (1974) 84–92.
- [37] C.W. Shu, Essentially non-oscillatory and weighted essentially non-oscillatory schemes for hyperbolic conservation laws, in: *Advanced Numerical Approximation of Nonlinear Hyperbolic Equations* (Cetraro, 1997), *Lecture Notes in Math.*, 1697, Springer, Berlin, 1998, pp. 325–432.
- [38] H. Struchtrup, The BGK model with velocity-dependent collision frequency, *Continuum Mech. Thermodyn.* 9 (1997) 23–31.